Simultaneous description of four positive parity bands and four negative parity bands

A. A. Raduta,[1,2] Al. H. Raduta,[2] and C. M. Raduta[2]
[1]*Department of Theoretical Physics and Mathematics, Bucharest University, P.O. Box MG11, Romania*
[2]*Department of Theoretical Physics, Institute of Physics and Nuclear Engineering, Bucharest, P.O. Box MG6, Romania*
(Received 4 June 2006; published 26 October 2006)

The extended coherent state model is further extended to describe two dipole bands of different parities. The formalism provides a consistent description of eight rotational bands. A unified description for spherical, transitional, and deformed nuclei is possible. Projecting out the angular momentum and parity from a sole state, the $K^\pi = 1^+$ band acquires a magnetic character, whereas the electric properties prevail for the other band. Signatures for a static octupole deformation in some states of the dipole bands are pointed out. Some properties that distinguish between the dipole band states and states of the same parity but belonging to other bands are mentioned. Interesting features concerning the decay properties of the two bands are found. Numerical applications are made for ^{158}Gd, ^{172}Yb, ^{228,232}Th, ^{226}Ra, ^{238}U, and ^{238}Pu, and the results are compared with the available data.

DOI: 10.1103/PhysRevC.74.044312 PACS number(s): 21.10.Re, 21.60.Ev, 27.80.+w, 27.90.+b

I. INTRODUCTION

The field of negative-parity bands became very attractive when the first suggestions for a static octupole deformation were advanced by Chasman [1] and Möller and Nix [2]. Because a nuclear shape with octupole deformation does not exhibit a space reflection symmetry and, conversely, a spontaneously broken symmetry leads to a new nuclear phase, one expects that the octupole deformed nuclei have specific properties. The main achievements of this field was reviewed in Refs. [3–5].

Identifying the nuclei that have static octupole deformation seems to be a difficult task. Indeed, because there is no measurable quantity for the octupole deformation, some indirect information about this variable should be found. Several properties are considered as signatures for octupole deformation: (a) In some nuclei like ^{218}Ra, the state 1^-, the head of the $K^\pi = 0^-$ band, has a very low position, and this is an indication that the potential energy has a flat minimum, as a function of the octupole deformation. (b) The parity-alternating structure in ground and the lowest 0^- bands suggests that the two bands may be viewed as being projected from a sole deformed intrinsic state, exhibiting both quadrupole and octupole deformations. (c) A nuclear surface with quadrupole and octupole deformations might have the center of charge in a different position than the center of mass, that results in having an electric dipole moment that may excite the state 1^- from the ground state, with a large probability. The list is not complete and thereby any new signature for this new nuclear phase deserves a special attention.

Few years ago we considered this subject within a phenomenological framework. Thus, in Refs. [6–10] we extended the coherent state model (CSM) [11,12] to the negative-parity bands. To the lowest positive-parity bands, named ground (g^+), beta (β^+), and gamma (γ^+), one associates three negative bands, g^-, β^-, γ^-, respectively. The six bands are obtained by projecting out the angular momentum and the parity from three orthogonal functions that exhibit both quadrupole and octupole deformations. An effective boson Hamiltonian is considered in the space of angular momentum and parity-projected states. The phenomenological boson model called the extended coherent state model (ECSM) has been successfully applied to a large number of nuclei, some of them suspected of exhibiting a static octupole deformation, whereas some of them are suspected to have vibrational octupole bands. Some signatures for a static octupole deformation in the excited bands have been pointed out.

In the present article we extend even more the coherent state model by adding a new pair of parity partner bands. These are characterized by $K^\pi = 1^+$ and $K^\pi = 1^-$. Also two new terms are added to the model Hamiltonian without altering its effective character, whose strength are fixed by fitting some particular data for the new bands.

The new extension is presented according to the following plan. In Sec. II, a brief description of the CSM and ECSM is given. The scope consists in having a self-standing work and in collecting the necessary definitions and notations. In Sec. III, the ingredients of the new extension are presented in extenso, i.e., the properties of the states that enlarge the model boson space as well as the corrective terms of the model Hamiltonian and their matrix elements are analytically given. In Sec. IV, we discuss the numerical application for seven nuclei. Because some results for ^{172}Yb and ^{226}Ra were reported in two earlier publications, here we consider only the new results. A summary of the results and the final conclusions are presented in Sec. V.

II. BRIEF REVIEW OF THE COHERENT STATE MODEL AND ITS EXTENDED VERSION

A. The coherent state model

In the beginning of 1980s, one of the present authors (A.A.R) proposed, in collaboration, a phenomenological model to describe the main properties of the first three collective bands i.e., ground, β, and γ bands [11,12]. The model space was generated through a projection procedure

from three orthogonal deformed states. The choice was made so that several criteria required by the existent data are fulfilled. The states are built up with quadrupole bosons and therefore we are dealing with those properties that are determined by the collective motion of the quadrupole degrees of freedom.

We suppose that the intrinsic ground state is described by a coherent state of Glauber type corresponding to the zeroth component of the quadrupole boson operator $b_{2\mu}$. The other two generating functions are the simplest polynomial excitations of the intrinsic ground state, chosen in such a way that the orthogonality condition is satisfied before and after projection. To each intrinsic state one associates an infinite rotational band. In two of these bands the spin sequence is $0^+, 2^+, 4^+, 6^+, \ldots$ etc., and therefore they correspond to the ground (the lowest one) and to the β bands, respectively. The third one involves all angular momenta larger or equal to 2 and describes, in the first order of approximation, the γ band. The intrinsic states depend on a real parameter d that simulates the nuclear deformation. In the spherical limit, i.e., d goes to zero, the projected states are multiphonon states of highest, second highest, and third highest seniority, respectively. In the large deformation regime, conventionally called rotational limit ($d = 3$ means already a rotational limit), the model states behave like a Wigner function, which fully agrees the behavior prescribed by the liquid drop model. The correspondence between the states in the spherical and rotational limits is achieved by a smooth variation of the deformation parameter. This correspondence agrees perfectly with the semiempirical rule of Sheline [13] and Sakai [14], concerning the linkage of the ground-, β- and γ- band states and the member of multiphonon states from the vibrational limit. This property is very important when one wants to describe the gross features of the reduced probabilities for the intra- and interband transitions.

In this restricted collective model space an effective boson Hamiltonian is constructed. A very simple Hamiltonian was found that has only one off-diagonal matrix element, namely one connecting the states from the ground and the γ bands.

$$H_{\mathrm{CSM}} = H_2' + \lambda \hat{J}_2^2,$$
$$H_2' = A_1(22\hat{N}_2 + 5\Omega_{\beta'}^\dagger \Omega_{\beta'}) + A_2 \Omega_\beta^\dagger \Omega_\beta, \qquad (1)$$

where $\hat{N}_2$ denotes the quadrupole boson number operator

$$\hat{N}_2 = \sum_{-2 \leqslant m \leqslant 2} b_{2m}^\dagger b_{2m}, \qquad (2)$$

whereas $\Omega_{\beta'}^\dagger$ and $\Omega_\beta^\dagger$ stand for the following second- and third-degree scalar polynomials:

$$\Omega_{\beta'}^\dagger = (b_2^\dagger b_2^\dagger)_0 - \frac{d^2}{\sqrt{5}},$$
$$\Omega_\beta^\dagger = (b_2^\dagger b_2^\dagger b_2^\dagger)_0 + \frac{3d}{\sqrt{14}}(b_2^\dagger b_2^\dagger)_0 - \frac{d^3}{\sqrt{70}}. \qquad (3)$$

The angular momentum carried by the quadrupole bosons is denoted by $\hat{J}_2$. The boson states space is spanned by the

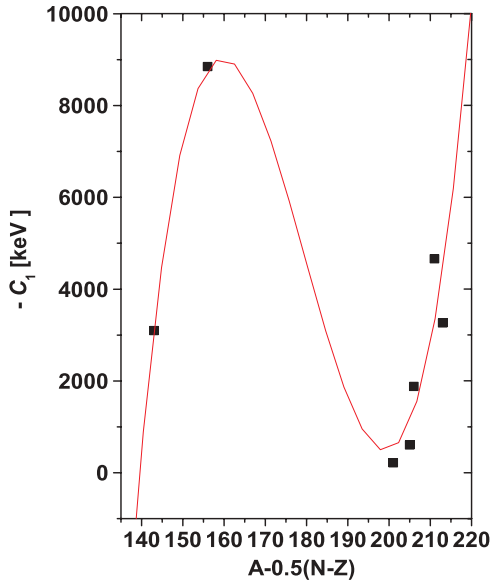

FIG. 1. (Color online) The structure coefficient $\mathcal{C}_1$, determined as explained in the text, is represented as function of $A - 0.5 * (N - Z)$ (black square). The obtained values are interpolated by a thid-order polynomial (full line curve).

projected states:

$$\varphi_{JM}^{(i)} = N_J^{(i)} P_{MK}^J \psi_i, \quad i = g, \beta, \gamma, \qquad (4)$$

where the intrinsic states are:

$$\psi_g = e^{d(b_{20}^\dagger - b_{20})}|0\rangle, \quad \psi_\beta = \Omega_\beta^\dagger \psi_g, \quad \psi_\gamma = \Omega_\gamma^\dagger \psi_g. \qquad (5)$$

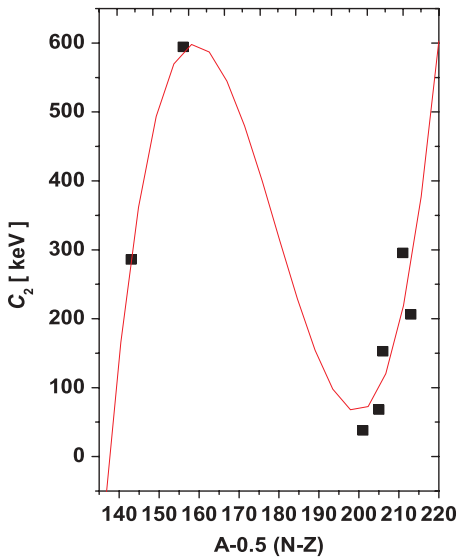

FIG. 2. (Color online) The structure coefficient $\mathcal{C}_2$, determined as explained in the text, is represented as function of $A - 0.5 * (N - Z)$ (black square). The obtained values are interpolated by a third-order polynomial (full line curve).

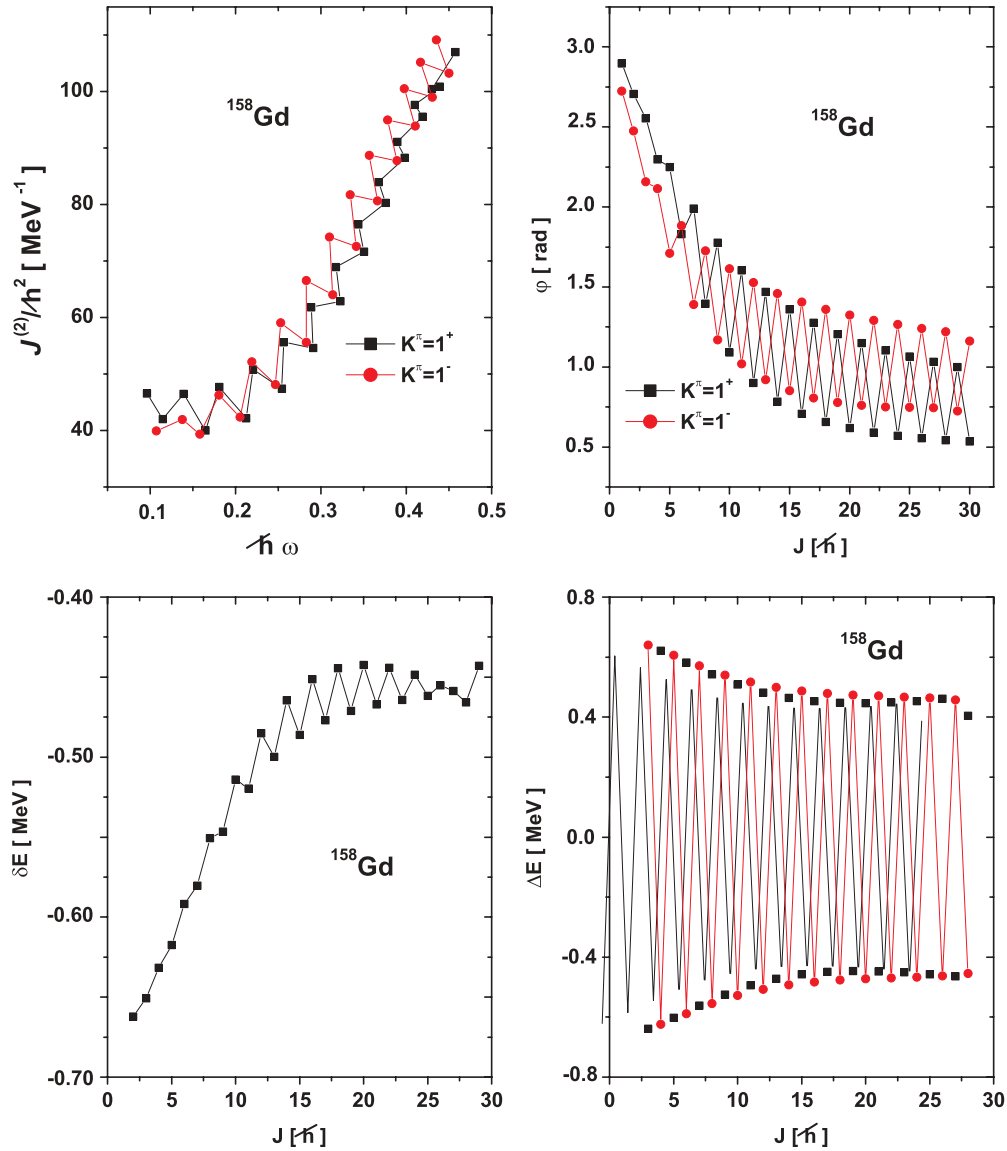

FIG. 3. (Color online) (Upper left panel) The dynamic moment of inertia is plotted as function of angular frequency. (Upper right panel) The angle between the angular momenta $\vec{J}_2$ and $\vec{J}_3$ is represented as function of angular momentum. (Low-left panel) The first-order energy displacement function is plotted vs. angular momentum. (Low-right panel) The second-order energy displacement is plotted as function of angular momentum. All theoretical results correspond to ^{158}Gd.

The excitation operator $\Omega^\dagger_\beta$ is given by Eq. (3), whereas the operator $\Omega^\dagger_\gamma$, which excites the γ-band states, is:

$$\Omega^\dagger_\gamma = (b^\dagger_2 b^\dagger_2)_{22} + d\sqrt{\frac{2}{7}} b^\dagger_{22}. \tag{6}$$

The angular momentum projection operator is defined by:

$$P^J_{MK} = \frac{2J+1}{8\pi^2} \int D^{J*}_{MK}(\Omega)\hat{R}(\Omega)d\Omega, \tag{7}$$

where the standard notations for the Wigner function and the rotation operator corresponding to the Eulerian angles Ω have been used.

The eigenvalues of the effective Hamiltonian in the restricted space of projected states have been analytically studied in both spherical and rotational limit. Compact formulas for transition probabilities in the two extreme limits have been also derived. This model has been successfully applied for a large number of nuclei from transitional and well-deformed regions. It is worth mentioning that by varying the deformation parameter and the parameters defining the effective Hamiltonian one can realistically describe nuclei satisfying various symmetries like SU(5) (Sm region) [15], O(6) (Pt region) [11,12], SU(3) (Th region) [16], and triaxial rotor (Ba, Xe isotopes) [17]. This model has been extended by including the coupling to the individual degrees of freedom [18]. In this way the spectroscopic

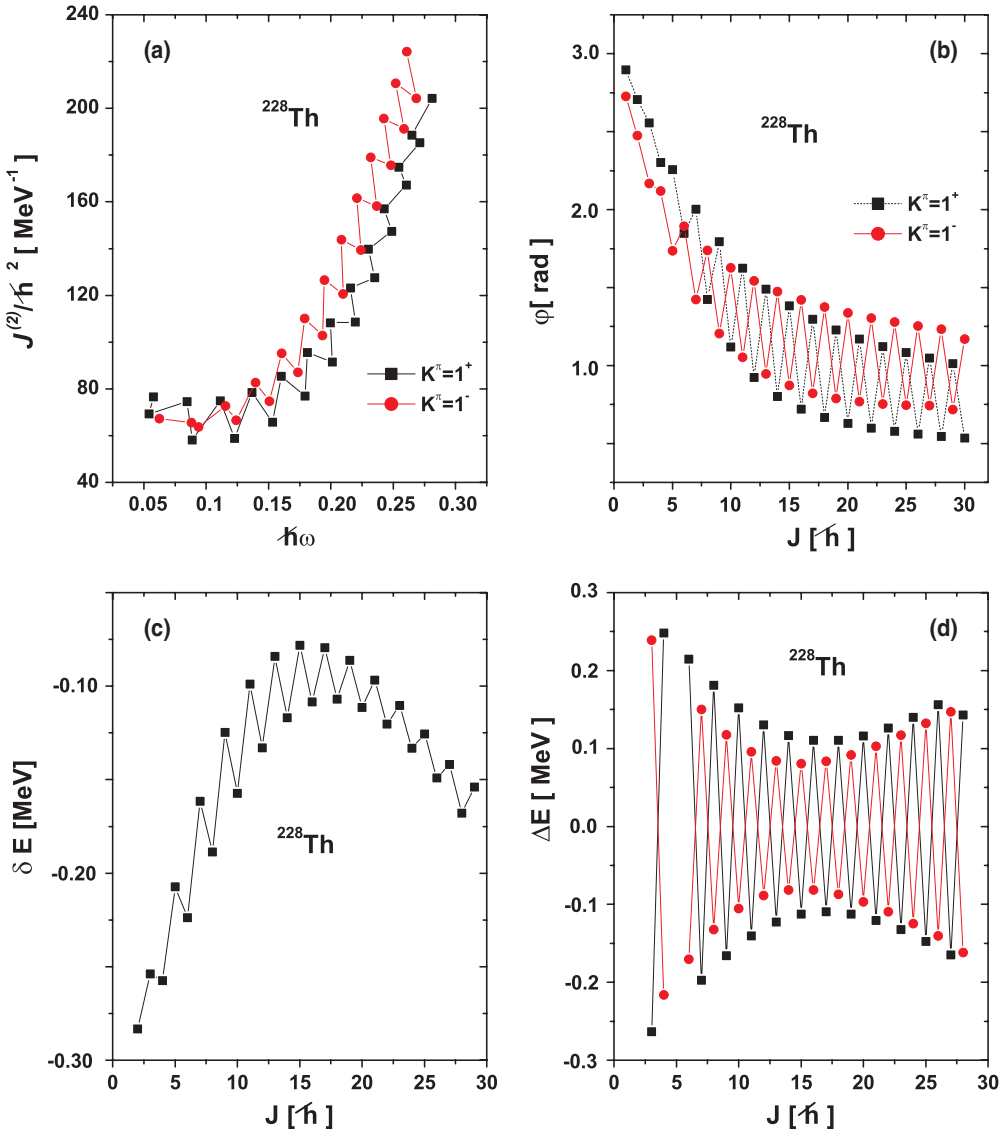

FIG. 4. (Color online) The same as in Fig. 3 but for ^{228}Th.

properties in the region of back-bending were quantitatively described.

The extension of the CSM formalism, which is presented here, considers a composite system of quadrupole and octupole bosons.

B. The extended coherent state model

The CSM formalism was generalized by assuming that the intrinsic ground state exhibits not only a quadrupole deformation but also an octupole one. Because the other bands, β and γ, are excited from the ground state, they also have this property. The octupole deformation is described by means of an axially symmetric coherent state for the octupole bosons $b^{\dagger}_{30}$. Thus, the intrinsic states for the ground, β, and γ bands are:

$$\Psi_g = e^{f(b^{\dagger}_{30}-b_{30})} e^{d(b^{\dagger}_{20}-b_{20})} |0\rangle_{(3)} |0\rangle_{(2)},$$
$$\Psi_\beta = \Omega^{\dagger}_{\beta}\Psi_g, \quad \Psi_\gamma = \Omega^{\dagger}_{\gamma}\Psi_g. \tag{8}$$

The notation $|0\rangle_{(k)}$ stands for the vacuum state of the 2^k-pole boson operators. Note that any of these states is a mixture of positive- and negative-parity states. Therefore they do not have good reflection symmetry. Due to this feature, the new extension of the CSM formalism has to project out not only the angular momentum but also the parity. The parity projection affects only the factor function depending on octupole bosons. Useful simplifications are achieved when this factor function is separately treated. The parity projected states are defined by:

$$\Psi^{(k)}_{\rm oc} = P^{(k)} e^{f(b^{\dagger}_{30}-b_{30})} |0\rangle_{(3)}, k = \pm, \tag{9}$$

where $P^{(k)}$ denotes the parity projection operator, which is defined by its property whereby, acting on a state consisting of a series of boson operators applied to the octupole vacuum, it selects only components with even powers in bosons if $k = +$ and odd components for $k = -$. From the parity-projected states one projects out, further, the components with good

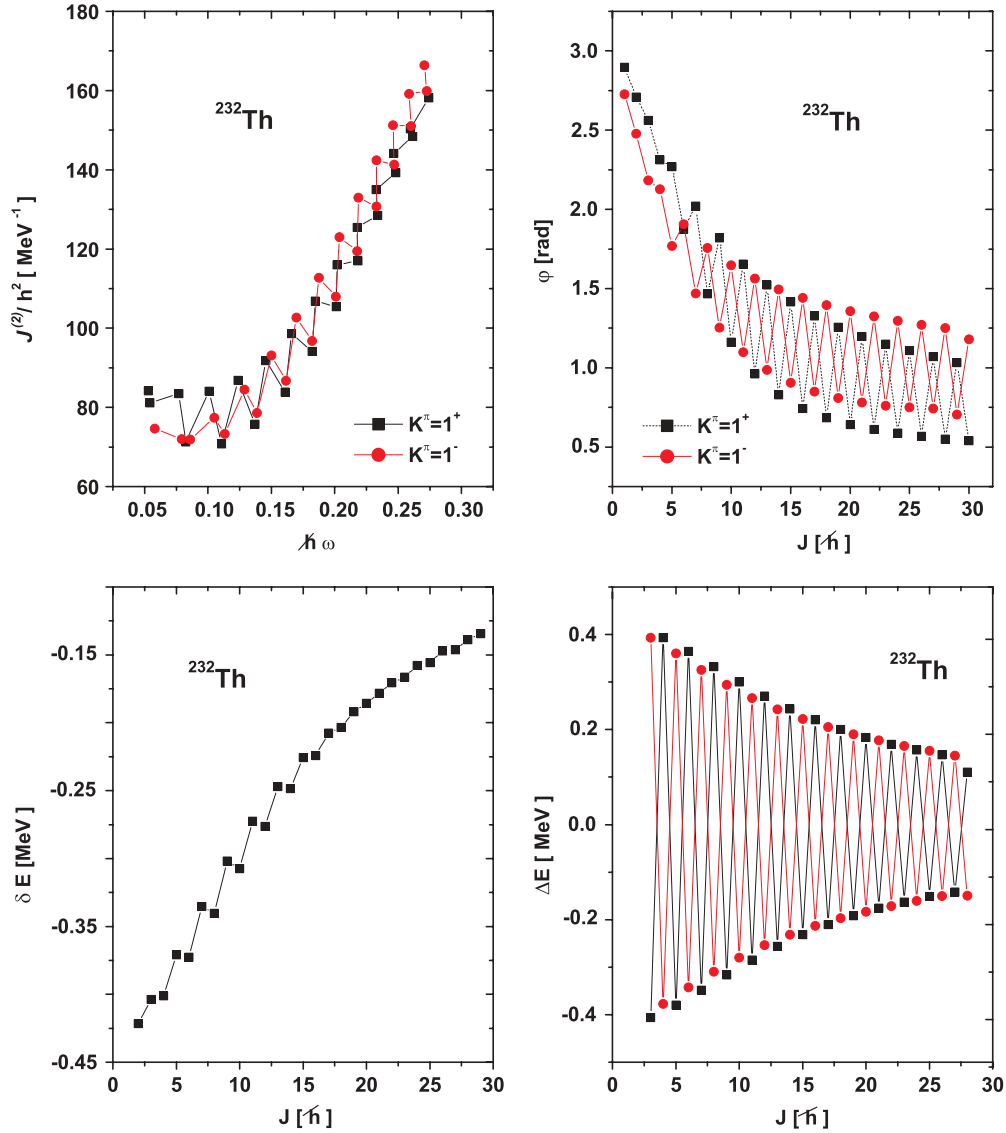

FIG. 5. (Color online) The same as in Fig. 3 but for ^{232}Th.

angular momentum:

$$\Psi^{(k)}_{\mathrm{oc};J_3M_3} = N^{(k)}_{\mathrm{oc};J_3} P^J_{M_30} \Psi^{(k)}_{\mathrm{oc}}. \tag{10}$$

The factor $N^{(k)}_{\mathrm{oc};J_3}$ assures that the projected state has the norm equal to unity. Its expression is given in Appendix A.

Then, the intrinsic states of good parity are defined by:

$$\Psi^{(k)}_i = \Psi^{(k)}_{\mathrm{oc}} \Psi_i, \quad i = g, \beta, \gamma, k = \pm. \tag{11}$$

The member states of ground, β, and γ bands are projected from the corresponding intrinsic states:

$$\varphi^{(i,k)}_{JM} = \mathcal{N}^{(i,k)}_J P^J_{MK_i} \Psi^{(k)}_i, \quad K_i = 2\delta_{i,\gamma}, \quad k = \pm; i = g, \beta, \gamma,$$
$$J = (\delta_{i,g} + \delta_{i,\beta})(\text{even}\,\delta_{k,+} + \text{odd}\,\delta_{k,-}) + \delta_{i,\gamma}(J \geqslant 2). \tag{12}$$

It can be shown that these projected states can be expressed by means of the octupole factor projected states and the projected states characterizing the CSM formalism.

$$\varphi^{(i,k)}_{JM} = \mathcal{N}^{(i,k)}_J \sum_{J_2,J_3} \left[N^{(k)}_{\mathrm{oc};J_3} N^{(i)}_{J_2}\right]^{-1} C^{J_3J_2J}_{0K_iK_i} \left[\Psi^{(k)}_{\mathrm{oc};J_3} \varphi^{(i)}_{J_2}\right]_{JM},$$
$$K_i = 2\delta_{i,\gamma}, \quad k = \pm; \quad i = g, \beta, \gamma, \tag{13}$$

The normalization factor has the expression:

$$\left[\mathcal{N}^{(i,k)}_J\right]^{-2} = \sum_{J_2,J_3} \left[N^{(k)}_{\mathrm{oc};J_3} N^{(i)}_{J_2}\right]^{-2} \left(C^{J_3J_2J}_{0K_iK_i}\right)^2,$$
$$K_i = 2\delta_{i,\gamma}, \quad k = \pm; \quad i = g, \beta, \gamma. \tag{14}$$

An effective boson Hamiltonian has been studied in the restricted collective space generated by the six sets of projected states. Note that from each of the three intrinsic states, one generates by projection two sets of states, one of positive and one of negative parity. When the octupole deformation goes to zero, the resulting states are just those characterizing the CSM model. In this limit we know already the effective

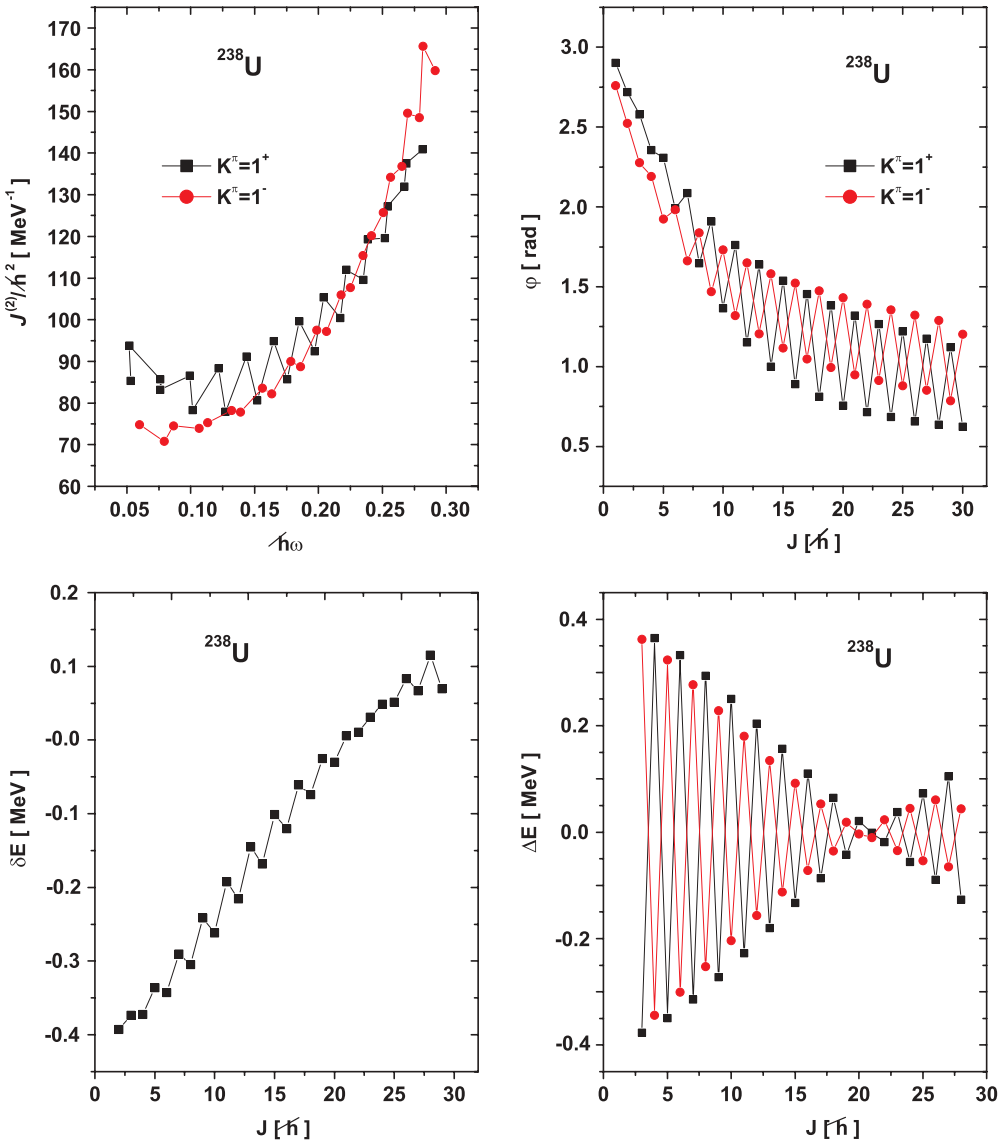

FIG. 6. (Color online) The same as in Fig. 3 but for ^{238}U.

quadrupole boson Hamiltonian. When the quadrupole deformation is going to zero the system exhibits vibrations around an octupole deformed equilibrium shape. We consider for the octupole Hamiltonian an harmonic structure because the non-harmonic octupole terms can be simulated by the quadrupole anharmonicities. As for the coupling between quadrupole and octupole bosons, we suppose that this can be described by a product between the octupole boson number operator, $\hat{N}_3$, and the quadrupole boson anharmonic terms that are involved in the CSM Hamiltonian. Indeed, it has been proved that including octupole anharmonicities in the coupling terms these terms provide an angular moment dependence for the corresponding matrix elements similar to the one already generated by the terms involving only the operator $\hat{N}_3$ in the coupling with the quadrupole bosons. Also, the scalar product of the angular momenta carried by the quadrupole ($\vec{J}_2$) and octupole bosons ($\vec{J}_3$), respectively, and the total angular momentum squared ($\vec{J}^2$) are included. Thus, the model Hamiltonian has the expression:

$$H = H_2' + \mathcal{B}_1\hat{N}_3(22\hat{N}_2 + 5\Omega^\dagger_{\beta'}\Omega_{\beta'}) + \mathcal{B}_2\hat{N}_3\Omega^\dagger_\beta\Omega_\beta + \mathcal{B}_3\hat{N}_3 + \mathcal{A}_{(J23)}\vec{J}_2\vec{J}_3 + \mathcal{A}_J\vec{J}^2. \quad (15)$$

Detail arguments in favor of this choice are presented in our previous publications on this subject. This Hamiltonian was used in Refs. [6–8] to study the ground and $K^\pi = 0^-$ bands. As shown in the quoted articles, the coupling term $\vec{J}_2\vec{J}_3$ is necessary to explain the low position of the state 1^- in the even-even Ra isotopes. Indeed, this term is attractive in the state 1^-, whereas for other angular momenta it is repulsive. Although this Hamiltonian has been introduced based on phenomenological ground, each of the terms involved can be microscopically obtained from a two-body interaction by using the boson expansion technique. This result can be found in one of our works [19], where the quadrupole-octupole interaction

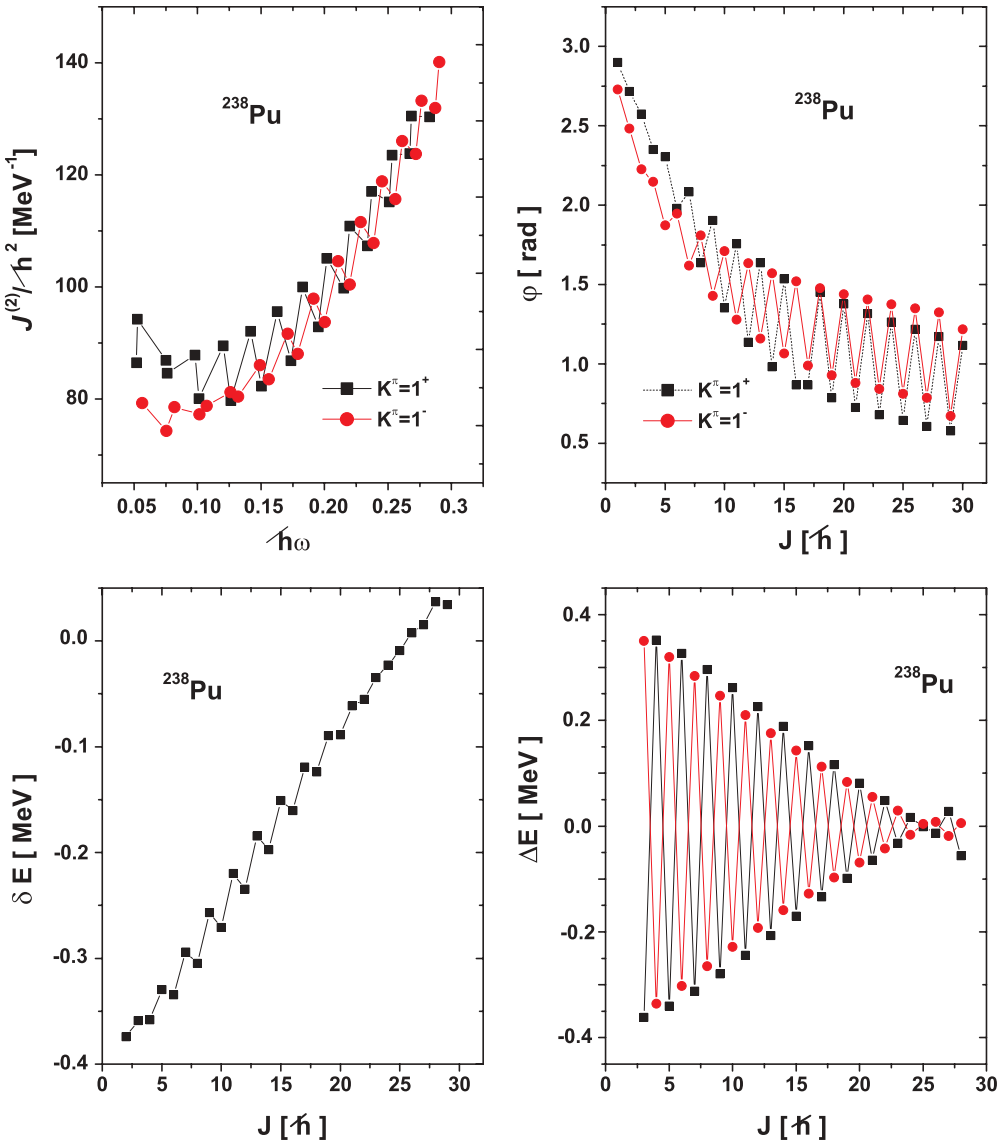

FIG. 7. (Color online) The same as in Fig. 3 but for ^{238}Pu.

was studied in terms of quadrupole and octupole QRPA (quasiparticle random phase approximation) boson operators.

Due to the specific structure of the CSM basis states the only nonvanishing off-diagonal matrix elements are those connecting the states of the ground and γ and of the 0^- and 2^- bands. The energies of the six bands are defined as eigenvalues of the model Hamiltonian in the model space of the projected states. They depend on the structure coefficients $\mathcal{A}_k[k = 1, 2, J, (J23)]$ and $\mathcal{B}_k, (k = 1, 3)$ defining the model Hamiltonian and the two deformation parameters, d and f. Therefore there are eight parameters that are to be determined, by fitting the data for excitation energies with the theoretical energies normalized to the ground-state energy. For the considered isotopes, the structure coefficients obtained in this manner have a smooth behavior when we change A or Z.

The connection between the present description and the rotational bands, as defined in the liquid drop model, was established in Ref. [14]. Indeed, as shown in Ref. [14] the projected states are linear superposition of states with definite K-quantum number. Moreover, in the asymptotic limit of the deformation parameter a single K prevails for each set of projected states, associated to the intrinsic unprojected states, respectively. Assigning to each band that K that labels the dominant component of the superposition quoted above, one may assert that the projected states, given by Eq. (13), comprises two $K^\pi = 0^+$, two $K^\pi = 0^-$, one $K^\pi = 2^+$, and one $K^\pi = 2^-$ subsets. Note that the K quantum number is equal to the eigenvalue of J_z, corresponding to the unprojected states Ψ_k with $k = g, \beta, \gamma$. Thus, the symmetry breaking in the wave functions given by Eq. (8) is equivalent to choosing an auxiliary intrinsic frame of reference.

The bands associated to these quantum numbers are conventionally denoted by $g^\pm(K^\pi = 0^\pm)$, $\beta^\pm(K^\pi = 0^\pm)$, and $\gamma^\pm(K^\pi = 2^\pm)$.

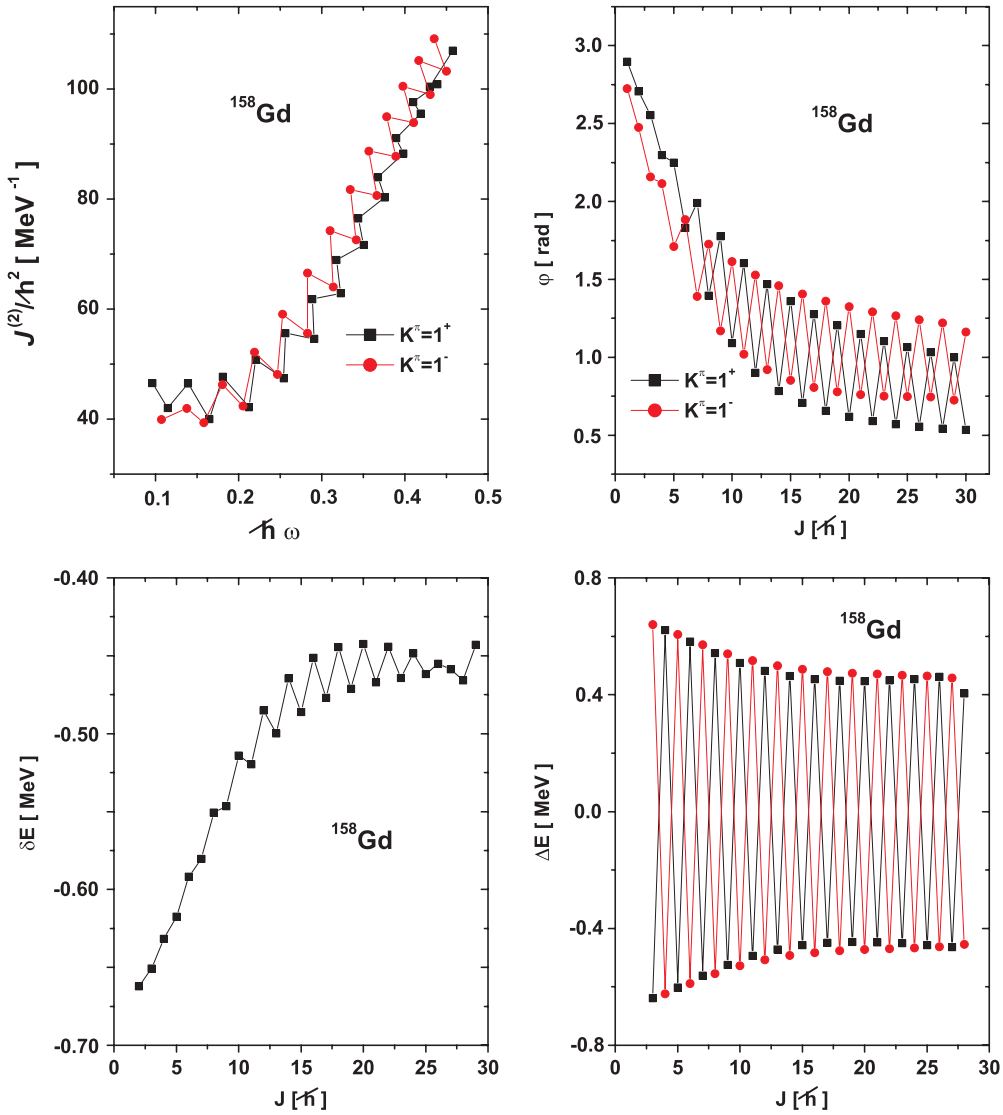

FIG. 8. (Color online) The angle between quadrupole and octupole angular momenta in the negative (up triangle) and positive (dagger) ground bands for the nuclei mentioned in the four panels.

III. THE DIPOLE BANDS

Extending further the ECSM formalism, by adding some new bands with keeping the basic principles of CSM unaltered, is a difficult task. Indeed, first one has to find an intrinsic state that is orthogonal onto other three states defined so far. Moreover, the orthogonality property has to be preserved also after projecting the angular momentum and parity. Suppose that this step has been already overcome. The next step is, then, to extend the model Hamiltonian by adding new terms that are mainly responsible for the description of the new states. The new Hamiltonian should be effective in the extended space of projected states, i.e., the off-diagonal matrix elements are either equal to zero or very small comparing them with the diagonal ones.

In the present article, we propose the following solution for the intrinsic state generating, through the angular momentum and parity projection, the member states of the dipole bands:

$$\Psi^{(1,\pm)} = \Omega_3^\dagger b_{31}^\dagger \Psi_{\rm oc}^{\mp} \Psi_g, \tag{16}$$

where

$$\Omega_3^\dagger = \left(b_3^\dagger b_3^\dagger\right)_0 + \frac{f^2}{\sqrt{7}}.$$

The states $\Psi^{(1,+)}$ and $\Psi^{(1,-)}$ are orthogonal because their scalar product involves the overlap of components with different number of bosons. Moreover, because $\Psi_{\rm oc}^{\pm}$ are vacuum states for the operator Ω_3, the intrinsic states for the dipole bands are orthogonal onto the intrinsic states associated with the bands $g^{\pm}$, $\beta^{\pm}$, $\gamma^{\pm}$. From these states one obtains two sets of angular momentum projected states:

$$\varphi_{JM}^{(1,\pm)} = \mathcal{N}_J^{(1,\pm)} P_{M1}^J \Psi^{(1,\pm)}, \tag{17}$$

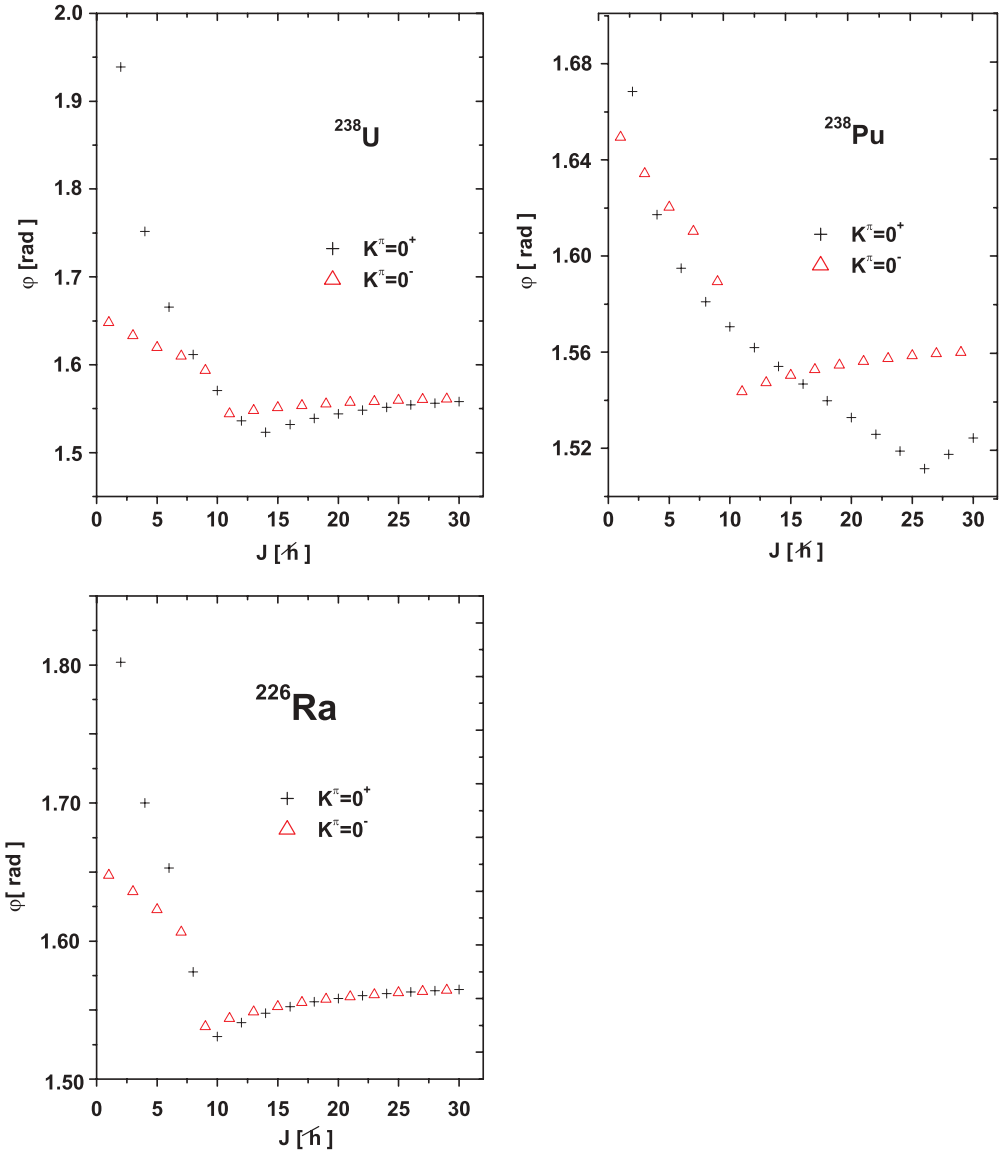

FIG. 9. (Color online) The same as described in the legend to Fig. 8 but for ^{238}U, ^{238}Pu, and ^{226}Ra.

with the projection operator defined by Eq. (7). The dipole projected state can be written in a tensorial form:

$$\varphi^{(1,\pm)}_{JM} = \mathcal{N}^{(1,\pm)}_{J} \sum_{J_2,J_3} C^{J_3\ J_2\ J}_{1\ \ 0\ \ 1} \left[N^{(\pm)}_{31;J} N^{(g)}_{J_2} \right]^{-1} \left[\varphi^{(\pm)}_{31,J_3} \varphi^{(g)}_{J_2} \right]_{JM}, \tag{18}$$

where the octupole factor state is defined by:

$$\varphi^{(1,\pm)}_{31;JM} = N^{(\pm)}_{31;J} P^{J}_{M1} \Omega^{\dagger}_{3} b^{\dagger}_{31} \Psi^{\mp}_{\rm oc}. \tag{19}$$

The norm factors $\mathcal{N}^{(1,\pm)}_{J}$, $N^{(\pm)}_{31;J}$ are analytically given in Appendix A.

It is worth to mention an useful property of the projected state defined above. Taking into account the expression of $\vec{J}_3$ in terms of octupole bosons:

$$J^{(3)}_{\mu} = \sqrt{12} \left[b^{\dagger}_{3} b_{3} \right]_{1\mu}, \tag{20}$$

one finds:

$$b^{\dagger}_{31} \Psi^{\mp}_{\rm oc} = \frac{1}{\mathcal{A}} J^{(3)}_{1} \Psi^{\pm}_{\rm oc}, \tag{21}$$

where

$$\mathcal{A} = -\sqrt{12} C^{3\ 3\ 1}_{1\ 0\ 1} f. \tag{22}$$

Commuting the angular momentum and the rotation operators, one arrives at the following expression for the octupole projected state:

$$\varphi^{(1,\pm)}_{31;JM} = N^{(\pm)}_{31;J} \frac{1}{\mathcal{A}} C^{J'\ 1\ J}_{0\ \ 1\ \ 1} \sum_{\mu,J'} C^{J'\ 1\ J}_{M'\ \mu\ M} J^{(3)}_{\mu} P^{J'}_{M'0} \Omega_3 \Psi^{\pm}_{\rm oc}. \tag{23}$$

Denoting the $K^{\pi} = 0^{\pm}$ projected state by:

$$\varphi^{(\pm)}_{3;JM} = N^{(\pm)}_{3;J} P^{J}_{M0} \Omega^{\dagger}_{3} \Psi^{\pm}_{\rm oc}, \tag{24}$$

the Eq. (23) leads to:

$$\varphi^{(1,\pm)}_{31;JM} = N^{(\pm)}_{31;J}\frac{1}{\mathcal{A}}C^{J\ 1\ J}_{0\ 1\ 1}\sqrt{J(J+1)}\left[N^{(\pm)}_{3;J}\right]^{-1}\varphi^{(\pm)}_{3;JM}. \quad (25)$$

Because the two projected states involved in the two sides of the above equation, respectively, are both normalized to unity we have:

$$\varphi^{(1,\pm)}_{31;JM} = \varphi^{(\pm)}_{3;JM},$$
$$\left[N^{(\pm)}_{31;J}\right]^{-1} = \frac{1}{\mathcal{A}}C^{J\ 1\ J}_{0\ 1\ 1}\sqrt{J(J+1)}\left[N^{(\pm)}_{3;J}\right]^{-1}. \quad (26)$$

This equation provides technical simplifications for calculating the matrix elements corresponding the dipole projected states.

Invoking the results obtained for the quantum number K, one can prove that the dipole projected states are $K^\pi = 1^\pm$ states, respectively. For a given J the projected states of positive and negative parity are obviously orthogonal onto each other. Moreover, they are orthogonal on the states of similar angular momentum describing the member states of the six bands that were previously defined.

The dipole projected states are weakly coupled to the states of other bands by the $\mathcal{B}_1$ and $\mathcal{B}_3$ terms of H (15). Moreover, these terms give large contribution to the diagonal matrix elements [20] involving the projected dipole states. Aiming at describing quantitatively the properties of the dipole states two terms are added to the model Hamiltonian.

$$\Delta H = \mathcal{C}_1\Omega_3^\dagger\Omega_3 + \mathcal{C}_2\Omega_3^\dagger\hat{N}_2\Omega_3. \quad (27)$$

The new terms affect only the diagonal matrix elements of the dipole states. Their strengths are fixed as follows: $\mathcal{C}_2$ is determined such that the corresponding contribution to the particular state energy, in the negative dipole band, cancels the one coming from the $\mathcal{B}_1$ term. $\mathcal{C}_1$ is fixed such that the measured excitation energy of the state 1^- is reproduced. With the new parameters determined in this way, the effect of the off diagonal matrix elements corresponding the $\mathcal{B}_1$ and $\mathcal{B}_3$ terms, on the energies in the two dipole bands amounts of a few keV. Due to this feature the energies of the two dipole bands are obtained as the corresponding average values of the model Hamiltonian, $H + \Delta H$.

IV. NUMERICAL RESULTS

A. Parameter description

The formalism presented in the previous section has been numerically applied for seven nuclei: ^{158}Gd, ^{172}Yb, ^{226}Ra, ^{228}Th, ^{232}Th, ^{238}U, ^{238}Pu. Because some results for ^{172}Yb and ^{226}Ra were earlier reported [21,22], for these nuclei we mention only the features not presented there. The experimental data are taken from Refs. [23–25] (^{158}Gd), [26–29] (^{172}Yb), [30–32] (^{226}Ra), [33] (^{228}Th), [32,34–36] (^{232}Th), [27,35,36] (^{238}U), [27,36,37] (^{238}Pu). Moreover, three pairs of parity partner bands have been treated in Refs. [9,10,12], where, excepting the new strengths $\mathcal{C}_1$ and $\mathcal{C}_2$, all parameters have been fixed through the least-squares procedure.

These new parameters have been fixed as explained in the previous section. Because the dipole-state energies are sensitive to changing $\mathcal{B}_1$ and $\mathcal{B}_3$, we change slightly the known values of these parameters to improve the agreement in the negative dipole band. However, changing the values of $\mathcal{B}_1$ and $\mathcal{B}_3$ affects some of calculated energies in the other six bands. Such corrections are washed out by a small change of one of the parameters $\mathcal{A}_J$, $\mathcal{A}_{J23}$. We have checked for few cases that the results obtained in this way are similar to those provided by a least-squares procedure applied for all eight bands. The final results for the model parameters are listed in Table I.

B. Dipole bands energies

As we have already suggested before, the calculated energies for $g^\pm, \beta^\pm, \gamma^\pm$ are practically the same as in Ref. [9,10,12] and therefore they are not given here. We stress the fact that the volume of explained data with the mentioned parameters is quite large. For example, in the previously treated six bands of ^{232}Th, about 55 excitation energies are known. Also, with the fixed deformation parameters, several experimental data concerning the transition reduced probabilities are realistically described. It is interesting to mention that these parameters have specific dependence on A and Z, which means that applying the formalism to new cases, the strength parameters can be considered fully determined

TABLE I. The deformation parameters d and f and the structure coefficients involved in the model Hamiltonian, obtained as described in the text, are listed for several isotopes. The deformations are dimensionless, while the remaining coefficients are given in units of keV.

	^{158}Gd	^{172}Yb	^{226}Ra	^{228}Th	^{232}Th	^{238}U	^{238}Pu
d	3.00	3.68	3.00	3.10	3.25	3.90	3.90
f	0.30	0.30	0.80	0.30	0.30	0.60	0.30
$\mathcal{A}_1$	21.49	26.94	20.29	17.72	14.26	20.64	18.84
$\mathcal{A}_2$	−12.28	−17.68	−17.21	−12.67	−8.34	−9.59	−8.63
$\mathcal{A}_J$	3.50	4.72	0.49	1.32	2.26	2.14	2.26
$\mathcal{A}_{J23}$	15.00	4.70	7.17	8.38	6.00	5.00	5.00
$\mathcal{B}_1$	−11.68	−24.29	−1.53	−2.79	−6.25	−11.97	−8.43
$\mathcal{B}_3$	3414.62	8327.68	523.07	858.37	2047.04	4483.28	3254.09
$\mathcal{C}_1$	−3096.52	−8853.24	−217.31	−603.58	−1879.04	−4663.88	−3265.85
$\mathcal{C}_2$	285.93	594.45	38.18	68.16	152.87	295.64	206.29

TABLE II. Experimental (left column) and theoretical (right column) excitation energies for the dipole band $K^\pi = 1^+$ states are given in units of MeV for the isotopes ^{158}Gd, ^{172}Yb, ^{228}Th, ^{232}Th.

J^+	^{158}Gd		^{172}Yb		^{228}Th		^{232}Th	
	Exp.	Th.	Exp.	Th.	Exp.	Th.	Exp.	Th.
1^+	2.534	2.531	2.010	1.880		1.247	1.489	1.508
2^+	2.539	2.563	2.047	1.897		1.250		1.519
3^+	2.631	2.638		1.970		1.311	1.561	1.567
4^+		2.698	2.073	1.984		1.301	1.573	1.578
5^+		2.829		2.133		1.426		1.673
6^+		2.927	2.156	2.139		1.409		1.687
7^+		3.108		2.368		1.595		1.827
8^+		3.256		2.370		1.587		1.851
9^+		3.470		2.676		1.818		2.029
10^+		3.681		2.683		1.832		2.073
11^+		3.911		3.056		2.092		2.276
12^+		4.189		3.078		2.139		2.347
13^+		4.423		3.506		2.412		2.567
14^+		4.771		3.552		2.497		2.669
15^+		5.001		4.023		2.774		2.899
16^+		5.417		4.101		2.899		3.033
17^+		5.636		4.606		3.174		3.628
18^+		6.118		4.719		3.338		3.435
19^+		6.323		5.251		3.606		3.672
20^+		6.870		5.403		3.808		3.871

TABLE IV. The same as in Table II, but for the $K^\pi = 1^-$ band.

J^-	^{158}Gd		^{172}Yb		^{228}Th		^{232}Th	
	Exp.	Th.	Exp.	Th.	Exp.	Th.	Exp.	Th.
1^-	1.856	1.856	1.155	1.155	0.952	0.952	1.078	1.078
2^-	1.895	1.912	1.198	1.207	0.968	0.989	1.100	1.110
3^-	1.978	1.970	1.222	1.257		1.017		1.140
4^-		2.091	1.331	1.375		1.104		1.213
5^-		2.184	1.353	1.443		1.142		1.257
6^-		2.366	1.541	1.636		1.281		1.372
7^-		2.500	1.567	1.716		1.330		1.428
8^-		2.727	1.828	1.986		1.512		1.582
9^-		2.911	1.849	2.077		1.578		1.654
10^-		3.165	2.193	2.421		1.791		1.839
11^-		3.404	2.209	2.524		1.880		1.931
12^-		3.672	2.630	2.935		2.113		2.140
13^-		4.970	2.646	3.053		2.227		2.255
14^-		4.237	3.134	3.523		2.470		2.479
15^-		4.598		3.661		2.613		2.619
16^-		4.857		4.182		2.860		2.854
17^-		5.281		4.342		3.033		3.021
18^-		5.526		4.906		3.277		3.261
19^-		6.013		5.091		3.481		3.456
20^-		6.240		5.692		3.719		3.699

from the previous analysis. As shown in Figs. 1 and 2, the new parameters $\mathcal{C}_1$ and $\mathcal{C}_2$ exhibit also a smooth dependence on the variable $A - 0.5(N - Z)$. Adding the third isospin component to A we avoided the situation when for the isotopes of the same A one obtains different values of the considered parameters, which results in having a ill-defined function. The calculated energies for the dipole bands are collected in Tables II–V. Only the states with angular momentum not larger than 20 are listed. Note that except for ^{172}Yb, [28,42] only few data

TABLE III. The same as in Table II but for ^{226}Ra, ^{238}U, ^{238}Pu.

J^+	^{226}Ra		^{238}U		^{238}Pu	
	Exp.	Th.	Exp.	Th.	Exp.	Th.
1^+		1.363	1.354	1.367	1.310	1.343
2^+		1.345		1.380		1.357
3^+	1.422	1.420		1.425		1.401
4^+		1.359		1.442		1.420
5^+		1.526		1.531		1.506
6^+		1.432		1.546		1.525
7^+		1.684		1.684		1.656
8^+	1.587	1.582		1.698		1.677
9^+		1.896		1.882		1.851
10^+		1.806		1.901		1.879
11^+		2.158		2.126		2.092
12^+		2.094		2.156		2.132
13^+		2.465		2.413		2.376
14^+		2.433		2.460		2.433
15^+		2.812		2.743		2.702
16^+		2.812		2.811		2.780
17^+		3.193		3.113		3.067
18^+		3.223		3.205		3.171
19^+		3.602		3.521		3.471
20^+		3.662		3.639		3.601

TABLE V. The same as in Table III but for the $K^\pi = 1^-$ band.

J^-	^{226}Ra		^{238}U		^{238}Pu	
	Exp.	Th.	Exp.	Th.	Exp.	Th.
1^-	1.080	1.049	0.967	0.967	0.963	0.863
2^-	1.102	1.090	0.988	0.998	0.986	0.992
3^-		1.108	1.035	1.033	1.019	1.025
4^-		1.211	1.053	1.100	1.083	1.089
5^-		1.227		1.153		1.138
6^-		1.394		1.259		1.240
7^-		1.409		1.326		1.302
8^-		1.631		1.472		1.443
9^-		1.647		1.553		1.516
10^-		1.913		1.736		1.695
11^-		1.933		1.831		1.781
12^-		2.233		2.048		1.994
13^-		2.258		2.157		2.093
14^-		2.584		2.405		2.336
15^-		2.619		2.529		2.450
16^-		2.962		2.802		2.719
17^-		3.012		2.942		2.851
18^-		3.365		3.237		3.140
19^-		3.434		3.392		3.291
20^-		3.790		3.707		3.597

are known for these bands. From the energy analysis, several common features can be seen. We note that in both $K^\pi = 1^-$ and $K^\pi = 1^+$ bands a doublet structure shows up. For us it is not clear whether this doublet structure is an indication of two bands of odd and even spins, respectively. This suspicion is somehow confirmed in ^{228}Th and ^{226}Ra, where in the low part of the spectrum the doublet members have not a natural energy ordering.

The excitation energies were further used to represent, in Figs. 3–7, the dynamic moment of inertia as function of angular frequency defined as:

$$\hbar\omega_I = \frac{dE}{dI} \approx \frac{1}{2}(E_I - E_{I-2}),$$
$$\frac{\mathcal{J}^{(2)}}{\hbar^2} = \left(\frac{d\hbar\omega}{dI}\right)^{-1} \approx \frac{2}{\hbar(\omega_I - \omega_{I-2})}. \tag{28}$$

The common feature of the moments of inertia is the zigzag structure in both the negative- and positive-parity bands. For the 1^+ band, the moments of inertia of odd and even spins are lying on smooth curves, respectively. The curve for the odd spins lies above that of even spins. The same is true also for the negative-dipole band with the difference that the curve corresponding to the even angular momenta is higher than that for odd values of angular momentum. Due to the relative position of the four curves comprising the moments of inertia of even and odd spin states of positive and negative parity, respectively, for some nuclei (^{172}Yb, ^{226}Ra, ^{238}U, and ^{238}Pu) it turns out that for some ranges of angular momenta the (odd, positive); (even, negative) and (even, positive); (odd, negative) states have moments of inertia lying on similar curves, respectively. This interleaved structure might be a signature for an octupole deformation in these states. To get a confirmation for such an expectation we plotted in the low panels of the above quoted figures the first- and second-order energy displacement functions defined as:

$$\delta E(J^-) = E(J^-) - \frac{(J+1)E[(J-1)^+] + JE[(J+1)^+]}{2J+1},$$
$$\Delta E_{1,\gamma}(J) = \frac{1}{16}[6E_{1,\gamma}(J) - 4E_{1,\gamma}(J) - 4E_{1,\gamma}(J) + E_{1,\gamma}(J) + E_{1,\gamma}(J)],$$
$$E_{1,\gamma}(J) = E(J+1) - E(J). \tag{29}$$

If the parity partner bands have a similar $J(J+1)$ pattern in a certain range of angular momentum, then the function δE is vanishing for J belonging to the mentioned range. The reverse statement, if valid, asserts that for the angular momenta where the first-order displacement function vanishes, the partner bands have identical moments of inertia, which further infers that the two bands can be viewed as being associated to a sole intrinsic state. However, the J dependence of the excitation energies for the considered nuclei deviates from the $J(J+1)$ law. If the energies can be described by a second-order polynomial in $J(J+1)$ and, moreover, the partner bands are characterized by the same strength for the $[J(J+1)]^2$ term, the second-order energy displacement function is vanishing. Conversely, if $\Delta E_{1,\gamma}$ is vanishing, this is a sign that the two partner bands have a similar $[J(J+1)]^2$ pattern. Concerning the second-order energy displacement function, one should mention that there are two distinct functions of angular momentum differing by the set of states involved. In one function the lowest state is 1^+ (the black squares), whereas for the other function the state 1^- is the lowest in energy. The parity assignment for the states involved in ΔE is conventionally taken as follows [43]. The states whose angular momenta differ by two units have the same parity, whereas those that differ by unity are of different parities. Inspecting Figs. 6 and 7 from the present article, Fig. 3 of Ref. [21] and Fig. 2 of Ref. [22], we remark that for ^{172}Yb, ^{238}U, and ^{238}Pu the second-order energy displacements vanish for two to three consecutive values of angular momenta, whereas for ^{226}Ra this is zero or very close to zero for $I \geqslant 11$.

In the right upper corner of Figs. 3–7, we plotted the angle between the angular momenta carried by the quadrupole and octupole bosons, respectively in the dipole states of positive as well as of negative parity. Such angle is defined as:

$$\cos\varphi = \frac{\langle\varphi^{(k)}_{JM}|\vec{J}_2\cdot\vec{J}_3|\varphi^{(k)}_{JM}\rangle}{\sqrt{\langle\varphi^{(k)}_{JM}|\hat{J}_2^2|\varphi^{(k)}_{JM}\rangle\langle\varphi^{(k)}_{JM}|\hat{J}_3^2|\varphi^{(k)}_{JM}\rangle}}, \quad k = 1,+;1,-. \tag{30}$$

Note that this angle is a decreasing function of angular momentum and that the angles for odd and even spin states of positive parity, respectively, lie on smooth curves. The same is true for the angles characterizing the negative-parity band. Moreover, for $I \leqslant 7$ the curves for odd-spin states of positive parity and for even-spin states of negative parity are very close to each other. The same is valid for the curves of even spin and positive parity and odd spin states of negative parity. Similarly, one could calculate the angle between the two angular momenta in the other parity partner bands. In Figs. 8 and 9 we give the results for the bands 0^+ and 0^-. For these bands we did not consider the admixture with the γ-band states of similar angular momenta, because the numerical results for the isotopes considered, the mixing amplitudes are small. For a better presentation we omitted the state 0^+ where the angle is equal to π. The angles for the two bands exhibit minima that are achieved for different values of angular momenta. However, for ^{226}Ra and ^{238}U the two minima are almost equal to each other and are reached for close values of angular momenta. After reaching the minima the angles increase and approach the limit value of $\pi/2$ in both bands. In the remaining cases this limit is met first by the band 0^- and much later in the ground band. Let us comment on the states where the angular momenta determined by the quadrupole and octupole bosons, respectively, are perpendicular on each other, respectively. The system under such a state constitute a precursor of a chiral symmetry [44]. Indeed, we could imagine a system of nucleons moving around a phenomenological core described by the quadrupole-octupole boson Hamiltonian considered here. Suppose that the coupling of the particle and core subsystems is such that the angular momentum carried by particles, say $\vec{j}$, is perpendicular to the plane $(\vec{J}_2, \vec{J}_3)$. If the system energy corresponding to the situation when the set $(\vec{j}, \vec{J}_2, \vec{J}_3)$ form a right triad is degenerate with the energy corresponding to the situation when the three vectors define

TABLE VI. Calculated gyromagnetic factors for the states belonging to the dipole $K^\pi = 1^+$ (left column) and $K^\pi = 1^-$ (right column) bands are given in units of nuclear magneton μ_N, for ^{158}Gd, ^{172}Yb, ^{228}Th, ^{232}Th.

J	^{158}Gd		^{172}Yb		^{228}Th		^{232}Th	
	$K^\pi = 1^+$	$K^\pi = 1^-$	$K^\pi = 1^+$	$K^\pi = 1^-$	$K^\pi = 1^+$	$K^\pi = 1^-$	$K^\pi = 1^+$	$K^\pi = 1^-$
1	0.645	0.865	0.645	0.789	0.645	0.851	0.645	0.832
2	1.081	0.403	0.859	0.379	1.042	0.399	0.989	0.392
3	0.503	0.548	0.424	0.452	0.489	0.530	0.469	0.506
4	0.939	0.316	0.760	0.286	0.910	0.310	0.869	0.302
5	0.476	0.486	0.395	0.405	0.461	0.472	0.441	0.452
6	0.821	0.293	0.697	0.263	0.803	0.386	0.776	0.280
7	0.457	0.448	0.381	0.383	0.444	0.437	0.425	0.422
8	0.723	0.281	0.642	0.254	0.712	0.276	0.695	0.269
9	0.439	0.417	0.372	0.366	0.428	0.409	0.412	0.398
10	0.645	0.273	0.592	0.249	0.638	0.269	0.627	0.263
11	0.422	0.391	0.363	0.352	0.412	0.386	0.398	0.377
12	0.584	0.267	0.548	0.245	0.579	0.263	0.573	0.258
13	0.406	0.370	0.355	0.340	0.398	0.366	0.386	0.359
14	0.536	0.261	0.511	0.241	0.533	0.258	0.528	0.253
15	0.391	0.353	0.347	0.329	0.384	0.349	0.374	0.344
16	0.498	0.256	0.480	0.238	0.496	0.253	0.492	0.249
17	0.376	0.338	0.339	0.319	0.371	0.336	0.362	0.331
18	0.476	0.252	0.453	0.237	0.466	0.250	0.463	0.246
19	0.364	0.327	0.332	0.310	0.359	0.324	0.352	0.321
20	0.442	0.249	0.431	0.234	0.440	0.246	0.438	0.243

a left triad, one says that the system has a chiral symmetry. Of course, such a situation is an ideal picture and in practice one expects that the two energies are only approximatively degenerate. The symmetry breaking is expected to yield some properties that are specific for the new nuclear phase.

C. Electromagnetic transition probabilities

The $E1$ and $M1$ transitions are determined by the following transition operators:

$$
\begin{aligned}
E_{1\mu} &= T^{(h)}_{1\mu} + T^{(\mathrm{anh})}_{1\mu},\\
T^{(h)}_{1\mu} &= q_h \sum_{\mu_2,\mu_3} C^{3\ 2\ 1}_{\mu_3\ \mu_2\ \mu} \left(b^\dagger_{3\mu_3} + (-)^{\mu_3} b_{3,-\mu_3}\right)\\
&\quad \times \left(b^\dagger_{2\mu_2} + (-)^{\mu_2} b_{2,-\mu_2}\right),\\
T^{\mathrm{anh}}_{1\mu} &= [b^\dagger_3(\hat{J}_3\hat{J}_2)]_{1\mu} + [(\hat{J}_2\hat{J}_3)b_3]_{1\mu}, \qquad (31)\\
M_{1\mu} &= g_2(\hat{J}_2)_\mu + g_3(\hat{J}_3)_\mu\\
&\quad + g'_2\{[\hat{J}_2(b^\dagger_3 b^\dagger_3)_2]_{1\mu} + ((b_3b_3)_2\hat{J}_2)_{1\mu}\}\\
&\quad + g'_3\{[\hat{J}_3(b^\dagger_2 b^\dagger_2)_2]_{1\mu} + ((b_2b_2)_2\hat{J}_3)_{1\mu}\}.
\end{aligned}
$$

The reduced matrix elements[1] of interest for these operators are given analytically in Appendix C. Let us first discuss the magnetic properties of the dipole bands. First, we calculated the gyromagnetic factors for the states of the two bands by considering only the lowest-order boson terms in the expression of the $M1$ transition operator. In Ref. [45] we derived an expression for the $M1$ transition operator by quantizing its classical expression. The important result was that the gyromagnetic factors g_2 and g_3 were expressed in terms of the Hamiltonian structure coefficients. The values obtained for ^{238}U are:

$$g_2 = 0.371\ \mu_N, \quad g_3 = 2.266\ \mu_N. \qquad (32)$$

These values have been adopted for all nuclei considered here. The results are presented in Tables VI and VII. We remark that the gyromagnetic factor of the state 2^- is very close to the phenomenologically adopted value for nuclei in the ground state, i.e., Z/A. This value is met in the positive-parity band for the state 13^+. The gyromagnetic factor of even-spin states of positive parity is constantly much larger than those of negative parity. By contrary, the odd-spin states of positive and negative parity have close gyromagnetic factors. For $J \leqslant 5$ the odd-spin states of positive parity have gyromagnetic factors that are slightly larger than those characterizing the odd-spin states of negative parity. Starting with $J = 7$, the ordering of gyromagnetic factors of odd-spin states in the two bands is changed.

The transition from the band 1^+ to the ground band is caused by the anharmonic term of the transition operator, whereas the intraband transitions as well as the gyromagnetic factors have been calculated by using only the lowest-order boson terms. The factors g_2 and g_3 have been taken as mentioned before.

[1] Throughout this article the Rose convention for the Wigner Eckardt theorem is used [20].

TABLE VII. Gyromagnetic factors for the states belonging to the dipole $K^\pi = 1^-$ and $K^\pi = 1^+$ bands.

J	^{226}Ra		^{238}U		^{238}Pu	
	$K^\pi = 1^+$	$K^\pi = 1^-$	$K^\pi = 1^+$	$K^\pi = 1^-$	$K^\pi = 1^+$	$K^\pi = 1^-$
1	0.645	0.931	0.645	0.793	0.645	0.773
2	1.100	0.427	0.813	0.381	0.806	0.374
3	0.510	0.644	0.409	0.461	0.407	0.431
4	0.959	0.351	0.719	0.289	0.712	0.279
5	0.484	0.592	0.378	0.417	0.375	0.385
6	0.841	0.334	0.667	0.268	0.659	0.257
7	0.467	0.563	0.366	0.398	0.363	0.365
8	0.745	0.329	0.621	0.260	0.614	0.248
9	0.451	0.544	0.358	0.386	0.355	0.352
10	0.670	0.330	0.579	0.255	0.572	0.243
11	0.437	0.531	0.351	0.377	0.347	0.340
12	0.614	0.332	0.542	0.253	0.534	0.239
13	0.423	0.522	0.344	0.369	0.341	0.330
14	0.572	0.337	0.509	0.252	0.500	0.236
15	0.412	0.514	0.338	0.362	0.334	0.320
16	0.541	0.342	0.480	0.251	0.472	0.234
17	0.403	0.507	0.332	0.356	0.328	0.312
18	0.518	0.348	0.457	0.250	0.447	0.232
19	0.395	0.499	0.327	0.351	0.322	0.304
20	0.500	0.354	0.436	0.250	0.426	0.230

Therefore, the branching ratios for the $M1$ transitions:

$$R^{10}_{++} = \left[\frac{\langle\varphi^{(1,+)}_J||M_1||\varphi^{(g,+)}_{J+1}\rangle}{\langle\varphi^{(1,+)}_J||M_1||\varphi^{(g,+)}_{J-1}\rangle}\right]^2,$$
$$R^{11}_{++} = \left[\frac{\langle\varphi^{(1,+)}_J||M_1||\varphi^{(1,+)}_{J+1}\rangle}{\langle\varphi^{(1,+)}_J||M_1||\varphi^{(1,+)}_{J-1}\rangle}\right]^2, \qquad (33)$$
$$R^{11}_{--} = \left[\frac{\langle\varphi^{(1,-)}_J||M_1||\varphi^{(1,-)}_{J+1}\rangle}{\langle\varphi^{(1,-)}_J||M_1||\varphi^{(1,-)}_{J-1}\rangle}\right]^2,$$

are free of any adjustable parameter. The calculated values for these ratios are given in Tables VIII and IX. The branching ratios to the ground band have a minimum for $7 \leqslant J \leqslant 9$ and a maximum for $15 \leqslant J \leqslant 19$. Exceptions are for ^{238}U and ^{238}Pu, where the maximum values are reached for $J = 23$. The dominant ratios are those for odd values of angular momentum. The same is true for the intraband transition for the band 1^+.

By contrast, in the negative-parity band the ratios corresponding to even angular momenta prevail. One notices that for ^{158}Gd, R^{11}_{++} has a minimum value for $J = 9$, whereas R^{11}_{--} has a maximum for $J = 8$. These extreme values change from one nucleus to another. The dominant intraband $M1$ transitions for the band 1^+ are those from even-spin states. Moreover, they increase with the angular momentum. For example, for ^{232}Th the $B(M1)$ value is 0.25 μ_N^2 for $J = 2$ and 4.23 μ_N^2 for $J = 30$. As for the band 1^- the dominant transitions are those from odd-spin states. Indeed, for the isotope mentioned above the $B(M1)$ value increase from 0.45 for $J = 3$ to 2.06 μ_N^2 for $J = 29$. Except for the first transitions ($2^+ \to 1^+$) all others $B(M1)$ values are larger than the ones associated to negative-parity band. Due to these facts we say that the band 1^+ has a dominant magnetic character. It is worth noting that, although the collective magnetic states of scissors nature are determined by the angular vibration, in a scissors fashion, of the symmetry axis of the proton and neutron systems, that angle being quite small, here the angle between $\vec{J}_2$ and $\vec{J}_3$ (which might be assimilated with the angle between the axis of the maximal moments of inertia of the quadrupole and octupole

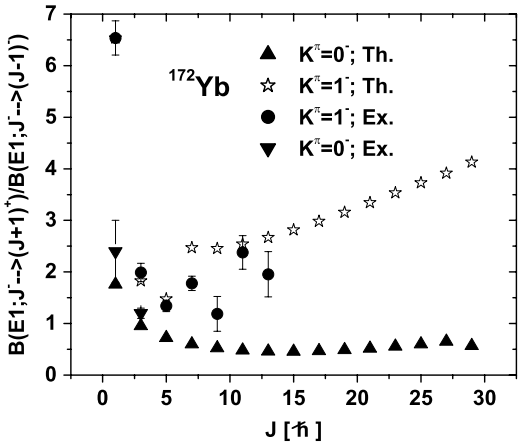

FIG. 10. The experimental branching ratios for the bands $K^\pi = 1^-$ (black circle) and $K^\pi = 0^-$ (down triangle) in ^{172}Yb are given as function of angular momentum. For comparison the calculated branching ratios, represented by stars and up triangles, respectively, are given as function of angular momentum. The transition operator involves the anharmonic term given by Eq. (31).

TABLE VIII. $M1$ branching ratios for the $K^\pi = 1^+$ and $K^\pi = 1^-$ bands for ^{158}Gd, ^{172}Yb, ^{228}Th, ^{232}Th.

J	^{158}Gd			^{172}Yb			^{228}Th			^{232}Th		
	$1^+ \to 0^+$	$1^+ \to 1^+$	$1^- \to 1^-$	$1^+ \to 0^+$	$1^+ \to 1^+$	$1^- \to 1^-$	$1^+ \to 0^+$	$1^+ \to 1^+$	$1^- \to 1^-$	$1^+ \to 0^+$	$1^+ \to 1^+$	$1^- \to 1^-$
1	0.376			0.369			0.375			0.373		
2			7.72			4.272			6.819			5.838
3	0.348	11.51		0.343	639.1		0.347	15.740		0.346	27.233	
4			20.45			6.335			15.802			11.561
5	0.160	5.22		0.185	21.14		0.164	6.144		0.170	8.015	
6			97.87			12.495			58.746			33.428
7	0.004	4.17		0.037	9.755		0.008	4.613		0.015	5.446	
8			2326			27.790			465.40			139.730
9	0.300	4.00		0.024	6.998		0.214	4.262		0.128	4.743	
10			978.40			72.40			8901			2025
11	3.114	4.15		0.478	5.979		2.275	4.302		1.466	4.595	
12			223.83			258.3			410.81			2105
13	23.821	4.45		2.535	5.574		15.494	4.524		8.870	4.691	
14			122.40			2548			172.680			353.600
15	549.200	4.84		11.065	5.455		189.61	4.848		66.498	4.916	
16			87.86			6013.			110.845			173.600
17	506.600	5.28		60.088	5.493		1629	5.238		1018	5.220	
18			71.37			680.7			84.690			116.470
19	108.700	5.77		1442	5.627		146.60	5.670		281.311	5.576	
20			61.92			294.14			70.747			90.154
21	60.940	6.28		624.060	5.825		70.577	6.133		94.363	5.968	
22			55.79			181.68			62.177			75.443
23	40.070	6.81		138.120	6.066		48.986	6.617		57.697	6.386	
24			51.42			132.16			56.352			66.146
25	37.760	7.36		73.400	6.345		39.639	7.118		43.756	6.825	
26			48.06			105.31			52.066			59.725
27	33.710	7.90		49.530	6.598		34.548	7.618		36.520	7.259	
28			45.68			91.05			49.189			55.694
29	31.070	8.41		37.290	6.768		31.257	8.082		31.951	7.649	
30			5.17			6.167			5.338			5.568

systems, respectively) is large. In this respect we could call the magnetic states from the band 1^+ shares like states.

Comparing the values of R^{11}_{++} with those describing the $M1$ branching ratios for the transitions relating the bands 1^- and 0^-, one finds out that the former ones prevail. The dominant

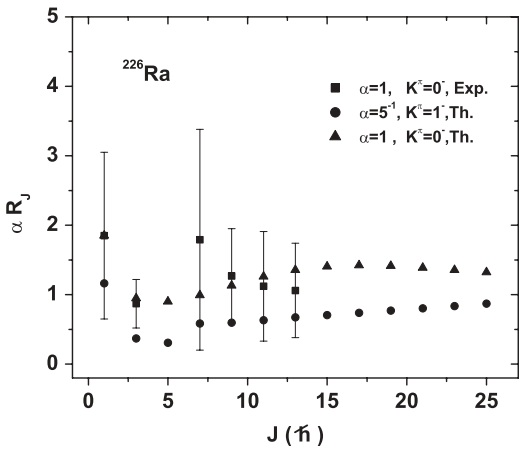

FIG. 11. The same as in Fig. 10 but for ^{226}Ra. For a better representation the results for the $K^\pi = 1^-$ band are divided by 5. The experimental data for this band are lacking.

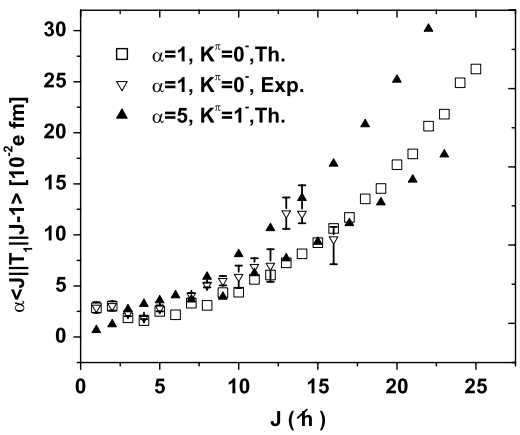

FIG. 12. The reduced matrix element for the electric dipole transition $J^- \to (J-1)^+$ with $J =$ odd and $J^+ \to (J-1)^-$ for $J =$ even.

TABLE IX. The same as in Table VIII but for ^{226}Ra, ^{238}U, ^{238}Pu.

J	^{226}Ra			^{238}U			^{238}Pu		
	$1^+ \to 0^+$	$1^+ \to 1^+$	$1^- \to 1^-$	$1^+ \to 0^+$	$1^+ \to 1^+$	$1^- \to 1^-$	$1^+ \to 0^+$	$1^+ \to 1^+$	$1^- \to 1^-$
1	0.376			0.368			0.368		
2			15.218			4.408			3.821
3	0.350	10.097		0.344	2820		0.343	1322	
4			222.04			6.857			5.144
5	0.165	4.760		0.192	37.780		0.190	42.575	
6			152.144			14.929			9.061
7	0.007	3.819		0.050	13.244		0.048	14.215	
8			29.201			41.279			17.435
9	0.220	3.640		0.006	8.489		0.007	8.989	
10			14.793			190.470			36.714
11	2.315	3.717		0.263	6.769		0.283	7.135	
12			10.067			1713			88.845
13	15.399	3.901		1.412	6.005		1.508	6.323	
14			7.908			416.900			282.240
15	171.476	4.127		5.457	5.652		5.888	5.959	
16			6.768			113.800			1951
17	2646	4.365		21.402	5.511		23.781	5.827	
18			6.134			58.266			7584
19	171.74	4.596		123.160	5.491		149.878	5.832	
20			5.786			37.904			1090
21	79.553	4.815		1569	5.547		1153	5.923	
22			5.612			27.941			411.090
23	54.482	5.017		443.440	5.651		355.806	6.073	
24			5.552			22.205			237.690
25	43.842	5.207		131.470	5.797		118.581	6.277	
26			5.566			18.540			165.700
27	38.210	5.383		68.750	5.896		64.481	6.430	
28			5.636			16.357			132.420
29	34.744	5.543		44.709	5.909		42.722	6.475	
30			0.469			1.318			6.480

ratios for the transitions $1^- \to 0^-$ are those corresponding to even values for the angular momentum.

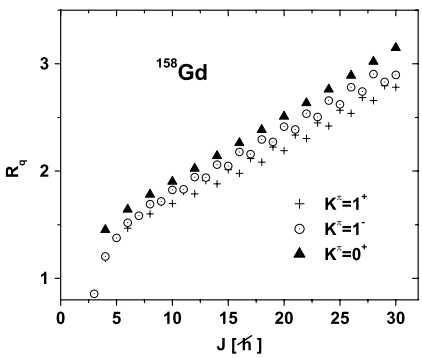

FIG. 13. The $B(E2)$ values for the intraband transitions for the $K^\pi = 1^+$ and $K^\pi = 1^-$ divided by the value corresponding to the transition $2^+_g \to 0^+_g$ are given as function of angular momentum. The ratio is denoted by R_q according to Eq. (35). For comparison, the intraband $B(E2)$ values characterizing the ground band are also given.

Now let us turn our attention to the electric transitions $E1$ and $E3$. In Tables X and XI we listed the calculated $E1$ branching ratios:

$$R^{10}_{+-} = \left[\frac{\langle\varphi^{(1,+)}_J||E_1||\varphi^{(g,-)}_{J+1}\rangle}{\langle\varphi^{(1,+)}_J||E_1||\varphi^{(g,-)}_{J-1}\rangle}\right]^2,$$
$$R^{10}_{-+} = \left[\frac{\langle\varphi^{(1,-)}_J||E_1||\varphi^{(g,+)}_{J+1}\rangle}{\langle\varphi^{(1,-)}_J||E_1||\varphi^{(0,+)}_{J-1}\rangle}\right]^2. \quad (34)$$

Concerning the ratio R^{10}_{-+}, two situations have been considered, namely when the transition operator is harmonic and when the anharmonic term defined above has been included. In that case we need the ratio $q_{\rm anh}/q_h$. These ratios are to be fixed so that a certain experimental data for the branching ratio is reproduced. Such experimental data are available for the cases of ^{172}Yb and ^{226}Ra and the determined values for the ratio of anharmonic and harmonic weights of the transition operator are equal to -1.722 and -1.4, respectively. The first value has been adopted also for ^{158}Gd, whereas the second value was assigned for the ratio characterizing the remaining nuclei considered here.

TABLE X. Calculated $E1$ branching ratios for the $K^\pi = 1^+$ and $K^\pi = 1^-$ bands in the isotopes for ^{158}Gd, ^{172}Yb, ^{228}Th, and ^{232}Th. Results given in the first and second columns are obtained with a harmonic structure for the transition operator, whereas those listed in the third column correspond to an anharmonic structure given by Eq. (31) with $q_{\rm anh}/q_h$ equal to -1.722 for ^{158}Gd and ^{172}Yb and -1.4 for Th isotopes. These values were obtained by fitting the experimental value corresponding to the state 1^- in ^{172}Yb and ^{226}Ra, respectively.

J	^{158}Gd			^{172}Yb			^{228}Th			^{232}Th		
	$1^+ \to 0^-$	$1^- \to 0^+$	$1^- \to 0^+$	$1^+ \to 0^-$	$1^- \to 0^+$	$1^- \to 0^+$	$1^+ \to 0^-$	$1^- \to 0^+$	$1^- \to 0^+$	$1^+ \to 0^-$	$1^- \to 0^+$	$1^- \to 0^+$
1		11.637	5.321		28.700	6.537		13.197	5.991		16.013	6.329
2	3.156			2.641			3.065			2.939		
3		1.948	1.871		2.056	1.828		1.955	1.869		1.974	1.858
4	1.559			1.299			1.512			1.448		
5		1.311	1.598		1.305	1.478		1.301	1.546		1.292	1.516
6	1.650			1.407			1.608			1.550		
7		7.144	2.899		8.280	2.470		7.163	2.967		7.290	2.849
8	2.221			1.935			2.177			2.112		
9		7.312	3.022		7.197	2.452		7.157	3.048		7.025	2.892
10	5.365			4.089			5.136			4.825		
11		8.294	3.252		7.252	2.539		7.976	3.252		7.624	3.058
12	5.909			4.415			5.627			5.255		
13		9.594	3.520		7.630	2.666		9.099	3.499		8.518	3.266
14	6.774			4.899			6.405			5.928		
15		11.115	3.808		8.194	2.816		10.429	3.768		9.603	3.498
16	7.815			5.453			7.336			6.726		
17		12.846	4.108		8.906	2.982		11.952	4.052		10.861	3.746
18	9.011			6.066			8.401			7.632		
19		14.771	4.417		9.742	3.158		13.652	4.346		12.276	4.005
20	10.356			6.737			9.597			8.644		
21		16.877	4.732		10.687	3.342		15.517	4.646		13.836	4.271
22	11.846			7.469			10.921			9.762		
23		19.152	5.050		11.732	3.532		17.537	4.951		15.532	4.542
24	13.480			8.279			12.373			10.988		
25		21.587	5.370		12.870	3.727		19.704	5.258		17.358	4.816
26	15.257			9.149			13.952			12.323		
27		23.944	5.686		13.646	3.915		21.755	5.560		19.008	5.085
28	17.188			10.128			15.676			13.789		
29		26.073	6.013		14.234	4.131		23.574	5.877		20.426	5.374
30												

In Fig. 10, the calculated branching ratios for the transitions of the negative dipole band to the ground band are compared with the corresponding data for the case [42] of ^{172}Yb. One notices a good agreement between the two sets of data. In Fig. 10 we also compare the calculated and experimental branching ratios for the band 0^-. One sees that these ratios are slowly decreasing with J up to $J = 11$ when a plateau is reached. By contrast, the branching for the dipole band decreases up to $J = 5$, has a small maximum at $J = 7$, a flat minimum at $J = 9$, and then is increases with J. Note that the dipole band has larger branchings than the band 0^-. One notes that although the two experimental ratios for the band 0^- are quite well described by those predicted by the Alaga rule, i.e., 2.0 and 1.33, respectively, large deviations from the Alaga rule are seen for the branching ratios characterizing the dipole band with $K^\pi = 1^-$. For example, for $J = 1$ and 3, the experimental ratios are about 6.5 and 2, respectively, whereas the predictions of the Alaga rule are 0.5 and 0.75. Our results and Alaga rule predictions are at variance not only in the region of low spin but also for high spin states. Indeed, for J larger than nine, the Alaga rule predictions are close to 0.9, whereas in our case, starting with $J = 9$, where the attained value is equal to about 2.5, our calculated ratios are increasing with J.

In Fig. 11 we compare three sets of data, namely the theoretical and experimental branching ratios characterizing the band 0^- and the branching ratio associated to the negative-parity dipole band in ^{226}Ra. For a better representation, the dipole branching ratios have been divided by 5. Remarkable the fact that modulo the factor 5, the calculated ratios for the two bands have similar behavior as function of J. It is interesting to see how the matrix elements of the $E1$ transition operator depend on the angular momentum for the bands with $K^\pi = 0^-$ and $K^\pi = 1^-$. Comparison of the two sets of matrix elements is made in Fig. 12. Note that for $J =$odd, the matrix element characterizes the transition from the states J^- to the state $(J-1)^+$, whereas for $J =$even, this links the states J^+ and $(J-1)^-$. For both situations an anharmonic structure for the transition operator has been considered. The parameters involved in the $T_{1\mu}$ operator have the values: $q_{\rm anh}/q_h = -1.4$

TABLE XI. Calculated $E1$ branching ratios for the $K^\pi = 1^+$ and $K^\pi = 1^-$ bands in the isotopes ^{226}Ra, ^{238}U, ^{238}Pu. Results given in the first and second columns are obtained with a harmonic structure for the transition operator, whereas those listed in the third column correspond to an anharmonic structure given by Eq. (31) with $q_{\rm anh}/q_h = -1.4$. This value was obtained by fitting the experimental value corresponding to the state 1^- in ^{226}Ra.

J	^{226}Ra			^{238}U			^{238}Pu		
	$1^+ \to 0^-$	$1^- \to 0^+$	$1^- \to 0^+$	$1^+ \to 0^-$	$1^- \to 0^+$	$1^- \to 0^+$	$1^+ \to 0^-$	$1^- \to 0^+$	$1^- \to 0^+$
1		10.500	5.815		37.24	8.036		39.380	8.072
2	3.141			2.518			2.521		
3		1.890	1.840		2.090	1.850		2.108	1.858
4	1.545			1.236			1.239		
5		1.294	1.523		1.321	1.443		1.325	1.449
6	1.635			1.344			1.347		
7		5.954	2.932		8.531	2.542		9.178	2.567
8	2.188			1.845			1.851		
9		6.104	2.988		7.178	2.460		7.569	2.484
10	5.100			3.742			3.778		
11		7.010	3.156		7.087	2.503		7.349	2.528
12	5.624			4.043			4.072		
13		8.402	3.364		7.326	2.591		7.502	2.619
14	6.464			4.474			4.498		
15		9.341	3.525		7.631	2.696		7.858	2.738
16	7.491			4.957			4.976		
17		10.375	3.688		8.079	2.817		8.364	2.875
18	8.510			5.467			5.497		
19		11.460	3.851		8.632	2.947		8.989	3.024
20	9.628			6.019			6.062		
21		12.554	4.015		9.269	3.085		9.715	3.182
22	10.827			6.612			6.670		
23		13.671	4.182		9.976	3.226		10.532	3.347
24	12.091			7.260			7.339		
25		14.807	4.356		10.741	3.369		11.430	3.518
26	13.412			7.965			8.069		
27		15.898	4.533		11.105	3.500		11.857	3.676
28	14.791			8.766			8.906		
29		16.945	4.718		11.371	3.657		12.149	3.875
30									

and $q_h = 10^{-2}$ fm. We note that the matrix elements describing the transition of the dipole state J^-, multiplied by a factor of 5, stays quite close to the similar matrix elements characterizing the band 0^-.

In Fig. 13 we study the intraband $E2$ transitions in the two dipole bands. The calculated $B(E2)$ values are divided by the $B(E2)$ value corresponding to the transition $2^+_g \to 0^+_g$.

$$R_q = \frac{B[E2; J \to (J-2)]}{B(E2; 2^+_g \to 0^+_g)}. \tag{35}$$

Results were obtained with a harmonic quadrupole transition operator and by neglecting the admixture of γ-band states in the structure of the ground-band states. For comparison, we also plotted the reduced transition probability in the ground band with a similar normalization. The intraband quadrupole transitions have similar dependence on angular momentum in the two dipole bands. Moreover, the $B(E2)$ values for the transitions $J^- \to (J-2)^-$ with J even lie close to the curve corresponding to the ground band.

The dipole bands may perform a $E3$ transition to the ground bands. To study the $E3$ properties of the dipole bands we have used an harmonic transition operator:

$$T_{3\mu} = q_3(b^\dagger_{3\mu} + (-)^\mu b_{3,-\mu}). \tag{36}$$

These transitions turns out to be weak. To have a flavor about the relative values of these transitions, comparing them to those from the band 0^-, we normalize each transition to the $B(E3)$ value associated for the transition $3^-_g \to 0^+_g$.

In Table XII we list the calculated values for the ratios:

$$T^{10}_{-+}(3; J) = \frac{B[E3, J^- \to (J+3)^+_g]}{B(E3; 3^-_g \to 0^+_g)},$$
$$T^{10}_{+-}(3; J) = \frac{B[E3, J^+ \to (J+3)^-_g]}{B(E3; 3^-_g \to 0^+_g)}. \tag{37}$$

TABLE XII. The calculated values for the $B(E3)$ values, normalized to the $B(E3)$ value for the transition $3^-_g \to 0^+_g$, are listed for the transitions of the dipole band states of angular momentum J to the states of angular momentum $(J+3)$ from the ground bands. The calculations were performed for ^{226}Ra.

J	$T^{10}_{-+}(3;J)$	$T^{10}_{+-}(3;J)$
1	0.002	
2		0.000
3	0.012	
4		0.011
5	0.030	
6		0.021
7	0.057	
8		0.036
9	0.090	
10		0.054
11	0.126	
12		0.076
13	0.163	
14		0.102
15	0.199	
16		0.133
17	0.234	
18		0.167
19	0.267	
20		0.205
21	0.297	
22		0.244
23	0.328	
24		0.284
25	0.358	
26		0.325
27	0.389	

V. CONCLUSIONS

In the previous sections we developed a formalism that appends the description of dipole bands to the extended coherent state model, which results in obtaining a simultaneous and consistent model of eight rotational bands, four of positive and four of negative parity. Because, for the seven nuclei considered, the results for three parity partner bands were already reported in some earlier publications, here we focus on the description of the dipole bands. The present article is the first devoted to the formalism description giving the analytical results describing the states and the matrix elements of the model Hamiltonian and transition operators.

The eight rotational bands are obtained by projecting out the angular momentum and parity from four intrinsic states that are quadrupole and octupole deformed functions and moreover orthogonal onto each other. By construction the four states have the property that the eight sets of projected states are all orthogonal. The model states depend on two real parameters that simulate the quadrupole and octupole deformation, respectively. In the spherical limit, i.e., both deformations tend to zero, specific multiphonon states of definite angular momentum, seniority, and number of bosons, respectively, are obtained. In the large deformation regime the projected states have a definite value for the K quantum number. In the restricted space of projected states, an effective quadrupole-octupole boson Hamiltonian is considered. Indeed, for the model Hamiltonian the only nonvanishing matrix elements are those involving the states $(J^\dagger_g, J^\dagger_\gamma)$ with $J =$ even and (J^-_g, J^-_γ) with $J =$ odd. The structure coefficients defining the model Hamiltonian as well as the deformation parameters have been fixed by fitting through the least square procedure the energies in the bands $g^\pm$, $\beta^\pm$, $\gamma^\pm$ and the energy of the head state in the $K^\pi = 1^-$ band. Also, one parameter ($\mathcal{C}_2$ has been determined so that the contribution of the $\mathcal{B}_3$ term to a particular state (2^-) is canceled. This condition seems to be sufficient to decrease the off-diagonal matrix elements involving the dipole band states to negligible values.

It is worth noting that dynamic moment of inertia of the odd and even angular momenta states lie on separate smooth curves, which could suggest that the two sets of states form distinct bands. This happens for both the positive- and negative-dipole bands. However, two pairs of these curves, one for positive and one for negative subsets of states, have an interleaved structure. These made us suspect that an octupole static deformation shows up. To confirm this suspicion we calculated the first-order and the second-order energy displacement functions. Both functions vanish for similar angular momenta in ^{172}Yb, ^{226}Ra, ^{238}U, and ^{238}Pu. The only isotope where the vanishing persists in a relatively long range of angular momentum is ^{228}Ra. For other nuclei mentioned above the vanishing takes place in one to three states. In Ref. [21] we interpreted the vanishing of the displacement function for a very short interval of J in a way that conciliates between the band intersection and static octupole deformation. Indeed, for such states it may be that they could be obtained by projection from an octupole deformed state that is different from the chosen model state for the dipole bands. Moreover, from this deformed state one could generate, through the angular momentum projection procedure, another two bands that are deformed all along and intersect the dipole bands considered here for the mentioned angular momentum. In this respect one could assert that bands intersection does not exclude the octupole deformation settlement.

Because the decay properties of the states depend on the corresponding boson structure, we calculated the angle between the angular momenta carried by the two kinds of bosons in the states of the ground bands, $g^\pm$. The result is that for high angular momentum states, this angle approaches the value $\pi/2$. This value is reached first in the negative and then in the positive band. Exception is for ^{226}Ra and ^{238}U where the angles in the two bands go simultaneously to the limit value $\pi/2$. We expect that for these systems, by adding a coupling set of particles, one could reach a chirally symmetric picture.

For the sake of a complete description of the dipole states of positive and negative parity, by using the eigenstates of the model Hamiltonian, the intra- and interband transitions of electric as well as of magnetic nature have been calculated.

Comparison with the experimental data is made in terms of the branching ratios of the negative-parity states. Also, these are compared with those characterizing the negative-parity band with $K^\pi = 0^-$. The gyromagnetic factors for the two bands were also calculated. One notices a strong dependence on angular momentum for the gyromagnetic factors.

Comparing the intraband $B(M1)$ values obtained for the two dipole bands, one concludes that the strength of magnetic transitions in the band $K^\pi = 1^+$ is larger than the one associated with the band $K^\pi = 1^-$. Due to this feature we say that the $K^\pi = 1^+$ band has a magnetic character. It is interesting to see whether the magnetic states studied in this article share a similar nature with the other known magnetic states. It is well established that the magnetic dipole states of scissors type [46] have energies smaller than 4 MeV and are excited by the orbital part of the magnetic dipole transition operator. They describe the angular oscillations, of a scissors fashion, for the proton and neutron systems' symmetry axes. The collective nature of these modes is confirmed by the fact that the total magnetic strength, in the range of 0–4 MeV, is proportional to the nuclear deformation squared [47]. Also, the energy depends on nuclear deformation. However, in Ref. [5] a sequence of magnetic states characterized by small or even vanishing deformation were identified in several nuclei. There, the collective magnetic nature is determined not by the nuclear deformation but by the angular momentum. The protons fill prolate orbitals, whereas the neutrons fill oblate orbitals. Moreover, the individual angular momenta for protons and neutrons are coherently summed up, respectively. The optimal energy state is met when the angle between the angular momenta for protons and neutrons are perpendicular onto each other. Due to this feature, these bands are called shares bands. Under certain circumstances, such a configuration asures a global spherical symmetry and a large total angular momentum. Recently, we studied microscopically the magnetic excitations that change the isospin of the system. The properties of such states are different from those of scissors states [48]. Of course the spin operator involved in the dipole magnetic transition operator may generate collective effects. The corresponding states are named magnetic spin-flip states and, in general, lie beyond the 4-MeV limit. Although they show up very seldom, the presence of the spin states below 4 MeV cannot be excluded (see, for example, Ref. [49]). In addition to the collective states mentioned above there are many two quasiparticle dipole states whose strengths are determined by the magnetic moments of the individual quasiparticles, participating in building up the dipole state. By contrast to all formalisms mentioned above, here the magnetic properties are not caused by the isospin degrees of freedom. Indeed, we do not distinguish between the proton and neutron bosons. Instead, we use two bosons of different multipolarity. In the present formalism the magnetic properties of the dipole states are determined by the angular momenta carried by the quadrupole and octupole boson systems, respectively. The quadrupole and octupole components rotate around a distinct axis, which makes an angle varying from about 170° in the state 1^+ to 57° for 29^+ and 36° in the state 30^+. Again, we mention that the angles characterizing the odd-spin states of positive parity lie on a smooth curve, whereas those for even-spin states stay on another smooth curve. This suggests that the two sets of states belong to distinct bands, which is consistent with the results for the dynamic moment of inertia of the dipole bands. Although in the state 1^+, the axis for quadrupole and octupole systems are close to each other but of different orientation, the motion is not of the scissors type, as can be seen from the associated branching ratio given in Tables VIII and IX. Indeed, the ratio $(1^+ \to 2_g^+)/(1^+ \to 0_g^+)$ varies from 0.368 to 0.376 for the isotopes considered here, which is smaller than the branching ratio characterising a scissors mode. We may conclude that the magnetic states belonging to the band $K^\pi = 1^+$ have a shares character and, moreover, characterize a deformed system. To decide whether the phenomenological model for the positive-parity dipole states provides a realistic description, more experimental data concerning the M_1 properties are necessary. These data would be a serious test for both the present model and the microscopic descriptions that assign to such states a two-quasiparticle character.

Concerning the $E1$ transition from the parity partner dipole bands to the $g^\pm$ bands, the strength characterizing the $K^\pi = 1^-$ band prevails over the one associated to the positive-parity band. Due to this feature we say that the band $K^\pi = 1^-$ has an electric nature. It is worth mentioning the role of parity projection in determining the magnetic or electric nature of the two bands.

Now let us say few words about the distinctive features of our formalism. The procedure is interesting not only because it is able to describe a relatively large volume of data with a relatively small number of parameters but also because it provides a consistent description of the rotational degrees of freedom. Indeed, all formalisms based on quadrupole and octupole boson interaction overestimate the contribution of the rotational degrees of freedom. That happens because in the intrinsic frame the Eulerian angles associated to the quadrupole and octupole coordinates are independent variables. Such a redundancy is automatically removed in the present formalism due to the projection operation. Another salient feature of the coherent state formalism is that it represents the ideal framework for the description of the semiclassical aspects of the collective motion. In particular, it provides a suitable description for the high-spin states, where the nuclear system behaves semiclassically, as well as for the quadrupole and octupole deformed systems.

Moreover our formalism provides an unified description of negative as well of positive-parity bands for both the spherical, transitional, and well-deformed nuclei.

Moreover, the mechanism for a static octupole deformation is different [12] from the traditional one where a fourth-order octupole boson term is necessary [38]. As explained in Ref. [12], in our formalism a second-order octupole boson term is sufficient for obtaining a stable octupole deformed shape.

An octupole-shaped system may have nonvanishing electric dipole moment. Also, due to the fact that the angular momentum is built up by both quadrupole and octupole bosons, one expects that the magnetic properties in a given state depend on its boson composition. Such properties may show up in dipole bands. Until now, the set on of the octupole deformation was associated with a jump in the dipole matrix element $J^- \to (J-1)_g^+$ (see the case of ^{226}Ra), where J^- belongs

to the band 0^-. We pointed out that the positive-parity state having static octupole deformation (the value of J where the energy displacement function vanishes) exhibit a large $M1$ branching ratio to the ground band. This, in fact, is a distinctive feature for the dipole bands, comparing them with the other pairs of parity partner bands. As mentioned, the angle between angular momenta carried by the quadrupole and octupole bosons, respectively, depends on the angular momentum of the dipole states in a specific manner.

It is worth investigating how the negative-dipole band compares to the the lowest negative-parity band, i.e., the $K^\pi = 0^-$ band. As shown in Figs. 10 and 11, the band 1^- is characterized by $E1$ branching ratios that are larger than those corresponding to the band 0^-. Moreover, as mentioned, the angle of angular momenta carried by the quadrupole and octupole bosons, respectively, have different dependences on the total angular momentum.

Before closing this section, we want to comment on the nature of the excited bands. Many authors believe that the states of nonvanishing K cannot be of a collective nature. To give an example, the authors of Ref. [28] invoke the arguments from Ref. [39] and interpret the dipole states of negative parity in ^{172}Yb as two quasineutron states. However, based on microscopic studies with surface δ interaction, the authors of Ref. [40] concluded that the $K^\pi = 1^-, 2^-$ bands of some actinides have, however, a collective nature. Actually, this is not the only example in the literature when one proves that the microscopic interpretation of the negative parity states, as two or four quasiparticle states, is not unique. Indeed, the double bending, one backward and one forward, seen in the ground and 0^- bands of ^{218}Ra, interpreted in Ref. [41] as caused by successive intersections of a collective band, a two-neutron and a two-neutron-plus-two-proton quasiparticle band, are fairly well reproduced by the phenomenological description provided by ECSM [9]. Although the dipole states for ^{172}Yb are considered in Ref. [28] as two quasineutron states, the branching ratios of the $K^\pi = 0^-, 1^-$ low-lying states are realistically described within an IBA-sdf formalism in Ref. [42]. Moreover, as we have already shown, the present article provides also a good description of the electric transitions in this nucleus. In the examples mentioned above the effect of single-particle degrees of freedom is simulated by the competition between various anharmonic terms involved in the model Hamiltonian or in the transition operator. More experimental data regarding both the excitation energies and transition probabilities in the dipole bands would be a decisive test for the predictive power of our formalism.

One should mention that many formalisms were devoted to the study of the negative-dipole bands. They are either phenomenological [37,42,50–52] or microscopic methods [39,40,53,54]. However, none of the quoted formalisms treat the dipole negative and positive bands on an equal footing. Moreover, the dipole negative bands are considered in isolation or, at best, together with a few adjacent bands. In contrast, the present formalism treats simultaneously eight rotational bands, four of positive and four of negative parity. Moreover, the treatment includes the region of high spin and the strongly deformed systems, a virtue that is lacking, for example, in the case of the popular formalism of IBA. Moreover, the two dipole bands are projected out from a sole function, exhibiting both quadrupole and octupole deformation. The magnetic and electric properties mixed up in the intrinsic function are separated due to the parity projection.

APPENDIX A

Here we list the explicit expressions for the norms of all projected states defined in the previous sections. The norm of the states obtained by projecting out the angular momentum and the parity from the octupole boson coherent state have the expression:

$$[N^{(\pm)}_{\mathrm{oc},J}]^{-2} = e^{-y_3}(2J+1)\mathcal{I}^{(\pm)}_J(y_3), \quad y_3 = f^2, \tag{A1}$$

where $\mathcal{I}^{(\pm)}$ stands for the overlap functions:

$$\begin{aligned}\mathcal{I}^{(+)}_J(y_3) &= \int_0^1 P_J(x) ch[f^2 P_3(x)]dx,\\ \mathcal{I}^{(-)}_J(y_3) &= \int_0^1 P_J(x) sh[f^2 P_3(x)]dx,\end{aligned} \tag{A2}$$

with $P_J(x)$ denoting the Legendre polynomial of rank J.

The norms of the dipole states are expressed in terms of norms characterizing the projected states associated to the quadrupole and octupole state factors:

$$\begin{aligned}[N^{(1,\pm)}_J]^{-2} &= \sum_{J_2,J_3}\left[N^{(\pm)}_{31;J_3}\right]^{-2}\left[N^{(g)}_{J_2}\right]^{-2}\left(C^{J_3\ J_2\ J}_{1\ 0\ 1}\right)^2,\\ \left[N^{(\pm)}_{31;JM}\right]^{-2} &= \frac{1}{\mathcal{A}}C^{J'\ 1\ J}_{0\ 1\ 1}\sqrt{J(J+1)}\,[N^{(\pm)}_{3,J}]^{-1},\\ \left[N^{(\pm)}_{3,J}\right]^{-2} &= [N^{(\pm)}_{\mathrm{oc},J}]^{-2}\left[2+\frac{4}{7}f^2\frac{\mathcal{I}^{(\pm)\prime}_J}{\mathcal{I}^{(\pm)}_J}\right],\\ \mathcal{A} &= -\sqrt{12}C^{3\ 3\ 1}_{1\ 0\ 1}f.\end{aligned} \tag{A3}$$

The standard notation for the Clebsch-Gordan coefficient $C^{j_1 j_2 j}_{m_1 m_2 m}$ has been used.

APPENDIX B

Here we give the analytical expressions for the matrix elements of the terms involved in the model Hamiltonian. For what follows it is useful to introduce the notation:

$${}^{(1)}X^{J_2J_3}_{Jk} = \left[N^{(1,k)}_J\right]^2\left[N^{(k)}_{31;J_3}N^{(g)}_{J_2}\right]^{-2}\left(C^{J_3\ J_2\ J}_{1\ 0\ 1}\right)^2. \tag{B1}$$

The final results for the matrix elements are:

$$\begin{aligned}\left\langle\varphi^{(1,\pm)}_{JM}\middle|\hat{N}_2\middle|\varphi^{(1,\pm)}_{JM}\right\rangle &= \sum_{J_2,J_3}{}^{(1)}X^{J_2J_3}_{J\pm}d^2\frac{I^{(1)}_{J_2}}{I^{(0)}_{J_2}},\\ \left\langle\varphi^{(1,\pm)}_{JM}\middle|\hat{N}_3\middle|\varphi^{(1,\pm)}_{JM}\right\rangle &= \sum_{J_2,J_3}\left\{2+\frac{18}{7}f^2\frac{\mathcal{I}^{(\pm)\prime}_{J_3}}{\mathcal{I}^{(\pm)}_{J_3}}\left[N^{(\pm)}_{\mathrm{oc};J_3}\right]^{-2}\right.\\ &\quad\left.+\frac{4}{7}f^4\sum_{J_1}\left(C^{J_1\ 3\ J_3}_{0\ 0\ 0}\right)^2\frac{\mathcal{I}^{(\mp)\prime}_{J_1}}{\mathcal{I}^{(\mp)}_{J_1}}\right.\end{aligned}$$

$$\times \left[N^{(\mp)}_{\text{oc};J_1}\right]^{-2}\Bigg\}\ {}^{(1)}X^{J_2J_3}_{J\pm}\left[N^{(\pm)}_{3;J_3}\right]^2$$

$$\left\langle\varphi^{(1,\pm)}_{JM}\middle|\hat{N}_2\hat{N}_3\middle|\varphi^{(1,\pm)}_{JM}\right\rangle = \sum_{J_2,J_3}\Bigg\{2+\frac{18}{7}f^2\frac{\mathcal{I}^{(\pm)'}_{J_3}}{\mathcal{I}^{(\pm)}_{J_3}}\left[N^{(\pm)}_{3;J_3}\right]^2 \times\left[N^{(\pm)}_{\text{oc};J_3}\right]^{-2}+\frac{4}{7}f^4\left(C^{J_1\ 3\ J_3}_{0\ 0\ 0}\right)^2 \times\frac{\mathcal{I}^{(\mp)'}_{J_1}}{\mathcal{I}^{(\mp)}_{J_1}}\left[N^{(\pm)}_{3;J_3}\right]^2\left[N^{(\mp)}_{\text{oc};J_1}\right]^{-2}\Bigg\} \times {}^{(1)}X^{J_2J_3}_{J\pm}d^2\frac{I^{(1)}_{J_2}}{I^{(0)}_{J_2}},$$

$$\left\langle\varphi^{(1,\pm)}_{JM}\middle|\vec{J}_2\vec{J}_3\middle|\varphi^{(1,\pm)}_{JM}\right\rangle = \sum_{J_2,J_3}{}^{(1)}X^{J_2J_3}_{J\pm}[J(J+1)-J_2(J_2+1) -J_3(J_3+1)], \tag{B2}$$

$$\left\langle\varphi^{(1,\pm)}_{JM}\middle|\Omega^\dagger\Omega\middle|\varphi^{(1,\pm)}_{JM}\right\rangle = \sum_{J_2J_3}\Bigg\{4+\frac{144}{49}f^2\frac{\mathcal{I}^{(\pm)'}_{J_3}}{\mathcal{I}^{(\pm)}_{J_3}}\left[N^{(\pm)}_{\text{oc},J_3}\right]^{-2} +\frac{16}{49}f^4\sum_{J'_3}\left(C^{J'_3\ 3\ J_3}_{0\ ;0\ ;0}\right)^2\frac{\mathcal{I}^{(\mp)'}_{J'_3}}{\mathcal{I}^{(\mp)}_{J'_3}} \times\left[N^{(\mp)}_{\text{oc},J'_3}\right]^{-2}\Bigg\}\ {}^{(1)}X^{J_2J_3}_{J\pm}\left[N^{(\pm)}_{3J_3}\right]^2, \tag{B3}$$

$$\left\langle\varphi^{(1,\pm)}_{JM}|\Omega^\dagger\hat{N}_2\Omega|\varphi^{(1,\pm)}_{JM}\right\rangle = \sum_{J_2J_3}\Bigg\{4+\frac{144}{49}f^2\frac{\mathcal{I}^{(\pm)'}_{J_3}}{\mathcal{I}^{(\pm)}_{J_3}}\left[N^{(\pm)}_{\text{oc},J_3}\right]^{-2} +\frac{16}{49}f^4\sum_{J'_3}\left(C^{J'_3\ 3\ J_3}_{0\ ;0\ ;0}\right)^2\frac{\mathcal{I}^{(\mp)'}_{J'_3}}{\mathcal{I}^{(\mp)}_{J'_3}} \times\left(N^{(\mp)}_{\text{oc},J'_3}\right)^{-2}\Bigg\}\ {}^{(1)}X^{J_2J_3}_{J\pm}\left[N^{(\pm)}_{3J_3}\right]^2d^2\frac{I^{(1)}_{J_2}}{I^{(0)}_{J_2}}.$$

APPENDIX C

The reduced matrix elements for the harmonic part of the $E1$ transition operator relating the dipole states to the states from the ground bands are:

$$\left\langle\varphi^{(1,+)}_J\middle|\middle|T^{(h)}_1\middle|\middle|\varphi^{(g,-)}_{J'}\right\rangle = q_1N^{(1,+)}_JN^{(g,-)}_{J'}\sum_{J_2,J_3,J'_2,J'_3}C^{J_3\ J_2\ J}_{1\ 0\ 0\ 1} \times C^{J'_3\ J'_2\ J'}_{0\ 0\ 0}\left[N^{(+)}_{31J_3}\right]^{-1}\left[N^{(g,-)}_{J'}\right]^{-1} \times\left\langle\varphi^{(+)}_{3,J_3}\middle||b^\dagger_3+b_3\middle|\varphi^{(-)}_{\text{oc};J'_3}\right\rangle \times\left\langle\varphi^{(g)}_{J_2}\middle||b^\dagger_2+b_2\middle|\varphi^{(g)}_{J'_2}\right\rangle,$$

$$\left\langle\varphi^{(1,-)}_J\middle|\middle|T^{(h)}_1\middle|\middle|\varphi^{(g,+)}_{J'}\right\rangle = q_1N^{(1,-)}_JN^{(g,+)}_{J'}\sum_{J_2,J_3,J'_2,J'_3}C^{J_3\ J_2\ J}_{1\ 0\ 0\ 1} \times C^{J'_3\ J'_2\ J'}_{0\ 0\ 0}\left(N^{(-)}_{31J_3}\right)^{-1}\left(N^{(g,+)}_{J'}\right)^{-1} \times\left\langle\varphi^{(-)}_{3,J_3}\middle||b^\dagger_3+b_3\middle|\varphi^{(+)}_{\text{oc};J'_3}\right\rangle \times\left\langle\varphi^{(g)}_{J_2}\middle||b^\dagger_2+b_2\middle|\varphi^{(g)}_{J'_2}\right\rangle,$$

$$\left\langle\varphi^{(+)}_{3,J_3}\middle||b^\dagger_3+b_3\middle|\varphi^{(-)}_{\text{oc};J'_3}\right\rangle = \frac{2}{\sqrt{7}}\frac{\hat{J}'_3}{\hat{J}_3}fN^{(+)}_{3;J_3}N^{(-)}_{\text{oc};J'_3} \times\left[N^{(-)}_{\text{oc};J_3}\right]^{-2}C^{J_3\ 3\ J'_3}_{0\ 0\ 0},$$

$$\left\langle\varphi^{(-)}_{3,J_3}\middle||b^\dagger_3+b_3\middle|\varphi^{(+)}_{\text{oc};J'_3}\right\rangle = \frac{2}{\sqrt{7}}\frac{\hat{J}'_3}{\hat{J}_3}fN^{(-)}_{3;J_3}N^{(+)}_{\text{oc};J'_3} \times\left[N^{(+)}_{\text{oc};J_3}\right]^{-2}C^{J_3\ 3\ J'_3}_{0\ 0\ 0}. \tag{C1}$$

The transition operator involves an anharmonic term, $T^{\text{anh}}_{1\mu}$. Due to this component of the transition operator a given state from a dipole band can decay to a state from the ground band of opposite parity:

$$\left\langle\varphi^{(1,\pm)}_J\middle||T^{\text{anh}}_1||\varphi^{(g,\mp)}_{J'}\right\rangle = N^{(1,\pm)}_JN^{(g,\mp)}_{J'}\left[N^{(\pm)}_{31;J_3}\right]^{-1}\left[N^{(g)}_{J_2}\right]^{-2} \times C^{J_3\ J_2\ J}_{1\ 0\ 1}C^{J'_3\ J_2\ J'}_{0\ 0\ 0} \times 5\sqrt{15J_2(J_2+1)J'_3(J'_3+1)} \times\hat{J}_2\hat{J}_3\hat{J}'_3\hat{J}'W(1113;22) \times W(J'_31J_33;J'_32) \times\sum_{J_4}(2J_4+1)W(J_3J_2J1;J_4J_2) \times W(J_3J_22J';J_4J'_3) \times W(J'2J1;J_41)\left\langle\varphi^{(\pm)}_{31;J_3}\middle||b^\dagger_3||\varphi^{(\mp)}_{\text{oc};J'_3}\right\rangle,$$

$$\left\langle\varphi^{(+)}_{3;J_3}\middle||b^\dagger_3+b_3\middle|\varphi^{(-)}_{\text{oc};J'_3}\right\rangle = \frac{2\hat{J}'_3f}{\sqrt{7}\hat{J}_3}N^{(+)}_{J_3}N^{(-)}_{\text{oc};J'_3}\left[N^{(+)}_{\text{oc};J^3}\right]^{-2}C^{J_3\ 3\ J'_3}_{0\ 0\ 0}. \tag{C2}$$

Taking for the $E2$ transition operator an harmonic form, the matrix elements describing the transitions within the dipole bands are:

$$\left\langle\varphi^{1,\pm}\middle\|b^\dagger_2+b_2\middle\|\varphi^{(1,\pm)}_{J'}\right\rangle = dN^{(1,\pm)}_JN^{(1,\pm)}_{J'}\hat{J}' \times\sum_{J_2J'_2J_3}C^{J_2\ J_3\ J}_{0\ 1\ 1}C^{J'_2\ J_3\ J'}_{0\ 1\ 1}C^{J'_2\ 2\ J_2}_{0\ 0\ 0}\hat{J}_2 \times W(2J_2J'J_3;J'_2J)\left[N^{(\pm)}_{31;J_3}\right]^{-1} \times\left\{\left[N^{(g)}_{J'_2}\right]^{-2}+\frac{2J'_2+1}{2J_2+1}\left[N^{(g)}_{J_2}\right]^{-2}\right\}. \tag{C3}$$

The $E3$ operator

$$T_{3\mu} = q_3\left[b^\dagger_{3\mu}+(-)^{1+\mu}b_{3-\mu}\right], \tag{C4}$$

relates a dipole state with a state from the corresponding ground band.

$$\left\langle\varphi^{(1,\mp)}_J\middle||T_3||\varphi^{(g,\pm)}_{J'}\right\rangle = q_3\frac{-2f}{\sqrt{7}}N^{(1,\mp)}_JN^{(g,\pm)}_{J'} \times\sum_{J_2,J_3,J'_3}\hat{J}'_3\hat{J}'C^{J_2\ J_3\ J}_{0\ 1\ 1}C^{J_2\ J'_3\ J'}_{0\ 0\ 0} \times C^{J_3\ 3\ J'_3}_{0\ 0\ 0}W(JJ_23J'_3;J_3J')\left(N^{(\mp)}_{31;J_3}\right)^{-1} \times\left(N^{(g)}_{J_2}\right)^{-2}N^{(\mp)}_{3;J_3}\left[N^{(\mp)}_{\text{oc};J_3}\right]^{-2}. \tag{C5}$$

The corresponding transition rate is compared with the octupole strength characterizing the transition $\varphi^{g,-} \to \varphi^{g,+}$.

$$\begin{aligned}\langle\varphi_J^{(g,-)}||b_3^\dagger + b_3||\varphi_{J'}^{(g,+)}\rangle &= f N_J^{(g,-)} N_{J'}^{(g,+)} \sum_{J_2,J_3,J_3'} C_{0\ 0\ 0}^{J_2\ J_3\ J} \\ &\times C_{0\ 0\ 0}^{J_2\ J_3'\ J'} C_{0\ 0\ 0}^{J_3'\ 3\ J_3} \hat{J}_3 \hat{J}' W\big(3 J_3' J J_2 \\ &; J_3 J'\big)\big[N_{J_2}^{(g)}\big]^{-2} \Big\{\big[N_{\mathrm{oc};J_3'}^{(+)}\big]^{-2} \\ &+ \frac{2J_3'+1}{2J_3+1}\big[N_{\mathrm{oc};J_3}^{(-)}\big]^{-2}\Big\}. \qquad \text{(C6)}\end{aligned}$$

The dipole states may decay to the ground band states of similar parity, by means of the $M1$ transition operator defined by Eq. (31).

The nonvanishing matrix elements relating the dipole and ground band states are:

$$\begin{aligned}\langle\varphi_J^{(1,+)}||M_1||\varphi_{J'}^{g,+)}\rangle &= g_2' N_J^{(1,+)} N_{J'}^{(g,+)} \sum C_{0\ 1\ 1}^{J_2\ J_3\ J} C_{0\ 0\ 0}^{J_2\ J_3'\ J'} \\ &\times \big[N_{31;J_3}^{(+)}\big]^{-1}\big[N_{J_2}^{(g)}\big]^{-1}\big[N_{\mathrm{oc};J_3'}^{(+)}\big]^{-1} \\ &\times \sqrt{J_2(J_2+1)}\, T_{JJ'}^{J_2 J_3} \\ &\times \langle\varphi_{3J_3}^{(+)}||(b_3^\dagger b_3^\dagger)_2||\varphi_{\mathrm{oc};J_3'}^{(+)}\rangle, \\ \langle\varphi_J^{(1,-)}\|M_1\|\varphi_{J'}^{g,-)}\rangle &= g_2' N_J^{(1,-)} N_{J'}^{(g,-)} \sum C_{0\ 1\ 1}^{J_2\ J_3\ J} C_{0\ 0\ 0}^{J_2\ J_3'\ J'} \\ &\times \big[N_{31;J_3}^{(-)}\big]^{-1}\big[N_{J_2}^{(g)}\big]^{-1}\big[N_{\mathrm{oc};J_3'}^{(-)}\big]^{-1} \\ &\times \sqrt{J_2(J_2+1)}\, T_{JJ'}^{J_2 J_3} \\ &\times \langle\varphi_{3J_3}^{(-)}||(b_3^\dagger b_3^\dagger)_2||\varphi_{\mathrm{oc};J_3'}^{(-)}\rangle, \qquad \text{(C7)}\end{aligned}$$

where

$$\begin{aligned}T_{JJ'}^{J_2 J_3} &= \hat{1}\hat{J}_2\hat{J}_3\hat{J}' \sum_{J_4}(2J_4+1) \\ &\times W(J_3' J_3 1 1; 2J_4) \\ &\times W(J_2 J_3' J 1; J' J_4) \\ &\times W(J_2 1 J J_3; J_2 J_4),\end{aligned}$$

$$\begin{aligned}\langle\varphi_{3J_3}^{(\pm)}\|(b_3^\dagger b_3^\dagger)_2\|\varphi_{\mathrm{oc};J_3'}^{(\pm)}\rangle &= \frac{4}{7} f^2 \hat{2}\hat{J}_3' N_{3J_3}^{(\pm)} N_{\mathrm{oc};J_3'}^{(\pm)} \\ &\times \sum_{J_1=\mathrm{odd}} C_{0\ 0\ 0}^{J_1\ 3\ J_3} C_{0\ 0\ 0}^{J_1\ 3\ J_3'\ J'} \\ &\times W(J_3' 2 J_1 3; J_3 3)\big[N_{\mathrm{oc};J_1}^{(\pm)}\big]^{-2}. \qquad \text{(C8)}\end{aligned}$$

As usual the abbreviation $\hat{J} = \sqrt{2J+1}$ is used. When one deals with the angular momentum operator, the hat suggests the operatorial character.

The $M1$ transitions within the dipole bands as well as the gyromagnetic factors of the dipole states were determined by restricting the transition operator to the lowest order boson terms:

$$M_{1\mu} = g_2(\hat{J}_2)_\mu + g_3(\hat{J}_3)_\mu. \qquad \text{(C9)}$$

The transition amplitudes are given by the reduced matrix elements:

$$\begin{aligned}\langle\varphi_J^{(1,\pm)}||g_2 J_2 + g_3 J_3||\varphi_{J'}^{(1,\pm)}\rangle &= N_J^{(1,\pm)} N_{J'}^{(1,\pm)} \sum_{J_2 J_3} C_{0\ 1\ 1}^{J_2\ J_3\ J} \\ &\times C_{0\ 1\ 1}^{J_2\ J_3\ J'}\big[N_{31;J_3}^{(+)}\big]^{-2}\big[N_{J_2}^{(g)}\big]^{-2} \\ &\times \big[\hat{J}_2\hat{J}' W(1 J_2 J' J_3; J_2 J) \\ &\times \sqrt{J_2(J_2+1)}\, g_2 + \hat{J}_3\hat{J}' \\ &\times W(1 J_3 J J_2; J_3 J') \\ &\times \sqrt{J_3(J_3+1)}\, g_3\big]. \qquad \text{(C10)}\end{aligned}$$

Using these expressions one could calculate the gyromagnetic factors of the dipole states:

$$g_J^\pm = \frac{1}{\sqrt{J(J+1)}}\langle\varphi_J^{(1,\pm)}||g_2\hat{J}_2 + g_3\hat{J}_3||\varphi_J^{(1,\pm)}\rangle. \qquad \text{(C11)}$$

[1] R. R. Chasman, Phys. Rev. Lett. **42**, 630 (1979); Phys. Lett. **B96**, 7 (1980).
[2] P. Möller and J. R. Nix, Nucl. Phys. **A361**, 117 (1981).
[3] S. G. Rohozinski, Rep. Prog. Phys. **51**, 541 (1988).
[4] P. A. Butler and W. Nazarewicz, Rev. Mod. Phys. **68**, 349 (1996).
[5] S. Frauendorf, Rev. Mod. Phys. **73**, 463 (2001).
[6] A. A. Raduta, Al. H. Raduta, and Amand Faessler, Phys. Rev. C **55**, 1747 (1997).
[7] A. A. Raduta, Al. H. Raduta, and Amand Faessler, J. Phys. G **23**, L49 (1997).
[8] A. A. Raduta, Amand Faessler, and R. K. Sheline, Phys. Rev. C **57**, 1512 (1998).
[9] A. A. Raduta, D. Ionescu, and Amand Faessler, Phys. Rev. C **65**, 064322 (2002).
[10] A. A. Raduta and D. Ionescu, Phys. Rev. C **67**, 044312 (2003).
[11] A. A. Raduta, V. Ceausescu, A. Gheorghe, and R. M. Dreizler, Phys. Lett. **B99**, 444 (1981); Nucl. Phys. **A381**, 253 (1982).
[12] A. A. Raduta, D. Ionescu, I. I. Ursu, and Amand Faessler, Nucl. Phys. **A720**, 43 (2003).
[13] R. K. Sheline, Rev. Mod. Phys. **32**, 1 (1960).
[14] M. Sakai, Nucl. Phys. **A104**, 301 (1967); Nucl. Data, Sec. A **8**, 323 (1970).
[15] A. A. Raduta and N. Sandulescu, Rev. Roum. Phys. **31**, 765 (1986).
[16] A. A. Raduta and C. Sabac, Ann. Phys. (NY) **148**, 1 (1983).
[17] U. Meyer, A. A. Raduta, and A. Faessler, Nucl. Phys. **A641**, 321 (1998).
[18] A. A. Raduta, C. Lima, and A. Faessler, Z. Phys. A **313**, 69 (1983).
[19] A. A. Raduta, V. Ceausescu, G. Stratan, and A. Sandulescu, Phys. Rev. C **8**, 1525 (1973).
[20] M. E. Rose, *Elementary Theory of Angular Momentum* (John Wiley & Sons, New York, 1957).
[21] A. A. Raduta, C. M. Raduta, and Amand Faessler, Phys. Lett. **B635**, 80 (2006).

[22] A. A. Raduta and C. M. Raduta, Nucl. Phys. **A768**, 170 (2006).
[23] M. Sugawara *et al*., Nucl. Phys. **A557**, 653c (1993).
[24] R. Bloch, B. Elbeck, and P. O. Tjom, Nucl. Phys. **A91**, 576 (1967).
[25] M. A. Lee, Nucl. Data Sheets **56**, 199 (1989).
[26] Y. Gono *et al*., Nucl. Phys. **A459**, 427 (1986).
[27] M. Gai, J. F. Ennis, M. Ruscev, E. C. Schloemer, B. Shivakumar, S. M. Sterbenz, N. Tsoupas, and D. A. Bromley, Phys. Rev. Lett. **51**, 646 (1983).
[28] P. M. Walker *et al*., Phys. Lett. **B87**, 339 (1979).
[29] S. Balraj, Nucl. Data Sheets **75**, 199 (1995).
[30] Y. A. Ellis-Akovali, Nucl. Data Sheets **69**, 155 (1993).
[31] H. J. Wollershein *et al*., Nucl. Phys. **A556**, 261 (1993).
[32] J. F. C. Cocks *et al*., Nucl. Phys. **A645**, 63 (1999).
[33] K. Hardt, P. Schueler, C. Guenther, J. Recht, K. P. Blume, and H. Wilzek, Nucl. Phys. **A419**, 34 (1984).
[34] R. S. Simon *et al*., Phys. Lett. **B108**, 87 (1982).
[35] J. G. Alessi, J. X. Saladin, C. Baktash, and T. Humanic, Phys. Rev. C **23**, 79 (1981).
[36] E. N. Shurshikov, Nucl. Data Sheets **53**, 601 (1988).
[37] C. M. Lederer, Phys. Rev. C **24**, 1175 (1981).
[38] R. V. Jolos and P. von Brentano, Phys. Rev. C **49**, 2301(R) (1994).
[39] K. Neergard and P. Vogel, Nucl. Phys. **A145**, 33 (1970).
[40] A. Faessler and A. Plastino, Z. Phys. **203**, 333 (1967).
[41] N. Schulz *et al*., Phys. Rev. Lett. **63**, 2645 (1989).
[42] P. von Brentano, N. V. Zamfir, and A. Zilges, Phys. Lett. **B278**, 221 (1992).
[43] D. Ionescu, Ph.D. thesis, IFIN-HH, Bucharest, 2003 (unpublished).
[44] S. Frauendorf, Z. Phys. **A358**, 163 (1997).
[45] A. A. Raduta, N. Lo Iudice, and I. I. Ursu, Nucl. Phys. **A608**, 11 (1996).
[46] N. Lo Iudice and F. Palumbo, Phys. Rev. Lett. **41**, 1532 (1978); G. D. Franceschi, F. Palumbo, and N. Lo Iudice, Phys. Rev. C **29**, 1496 (1984).
[47] W. Ziegler, C. Rangacharyulu, A. Richter, and C. Spieler, Phys. Rev. Lett. **65**, 2515 (1990).
[48] A. Aroua, M. S. Fayache, L. Zamick, Y. Y. Sharon, E. Moya de Guerra, P. Sarriguren, and A. A. Raduta, Nucl. Phys. **A728**, 96 (2003).
[49] A. A. Raduta, A. Escuderos, and E. M. de Guerra, Phys. Rev. C **65**, 024312 (2002).
[50] W. Donner and W. Greiner, Z. Phys. **197**, 440 (1966).
[51] H. J. Daley and B. R. Barret, Nucl. Phys. **A449**, 256 (1986).
[52] A. F. Barfield, B. R. Barret, J. L. Wood, and O. Scholten, Ann. Phys. (NY) **182**, 344 (1988).
[53] A. Y. Dzublik and V. Y. Denisov, Phys. At. Nucl. **56**, 477 (1993).
[54] E. Garrote, J. L. Egido, and L. M. Robledo, Phys. Lett. **B410**, 86 (1997); Phys. Rev. Lett. **80**, 4398 (1998).